DISCRETE AND CONTINUOUS MODELS AND APPLIED COMPUTATIONAL SCIENCE

Volume 28 Number 2 (2020)

Founded in 1993
Founder: PEOPLES' FRIENDSHIP UNIVERSITY OF RUSSIA

DOI: 10.22363/2658-4670-2020-28-2

Edition registered by the Federal Service for Supervision of Communications, Information Technology and Mass Media
Registration Certificate: ПИ № ФС 77-76317, 19.07.2019

ISSN 2658-7149 (online); 2658-4670 (print)
4 issues per year.
Language: English.

Publisher: Peoples' Friendship University of Russia (RUDN University).
Indexed in Ulrich's Periodicals Directory (http://www.ulrichsweb.com), in Russian Science Citation Index (https://elibrary.ru), EBSCOhost (https://www.ebsco.com), CyberLeninka (https://cyberleninka.ru).

Aim and Scope

Discrete and Continuous Models and Applied Computational Science arose in 2019 as a continuation of RUDN Journal of Mathematics, Information Sciences and Physics. RUDN Journal of Mathematics, Information Sciences and Physics arose in 2006 as a merger and continuation of the series "Physics", "Mathematics", "Applied Mathematics and Computer Science", "Applied Mathematics and Computer Mathematics".

Discussed issues affecting modern problems of physics, mathematics, queuing theory, the Teletraffic theory, computer science, software and databases development.

It's an international journal regarding both the editorial board and contributing authors as well as research and topics of publications. Its authors are leading researchers possessing PhD and PhDr degrees, and PhD and MA students from Russia and abroad. Articles are indexed in the Russian and foreign databases. Each paper is reviewed by at least two reviewers, the composition of which includes PhDs, are well known in their circles. Author's part of the magazine includes both young scientists, graduate students and talented students, who publish their works, and famous giants of world science.

The Journal is published in accordance with the policies of COPE (Committee on Publication Ethics). The editors are open to thematic issue initiatives with guest editors. Further information regarding notes for contributors, subscription, and back volumes is available at http://journals.rudn.ru/miph.

E-mail: miphj@rudn.ru, dcm@sci.pfu.edu.ru.

EDITORIAL BOARD

Computer Design: *A. V. Korolkova*

Address of editorial board:
Ordzhonikidze St., 3, Moscow, Russia, 115419
Tel. +7 (495) 955-07-16, e-mail: publishing@rudn.ru
Editorial office:
Tel. +7 (495) 952-02-50, miphj@rudn.ru, dcm@sci.pfu.edu.ru
site: http://journals.rudn.ru/miph

Paper size 70×1 00/16. Offset paper. Offset printing. Typeface "Computer Modern".
Conventional printed sheet 4,51. Printing run 500 copies. Open price. The order 445.
PEOPLES' FRIENDSHIP UNIVERSITY OF RUSSIA
6 Miklukho-Maklaya St., 117198 Moscow, Russia
Printed at RUDN Publishing House:
3 Ordzhonikidze St., 115419 Moscow, Russia,
Ph. +7 (495) 952-04-41; e-mail: publishing@rudn.ru

Discrete & Continuous Models

& Applied Computational Science

2020, 28 (2) 104

http://journals.rudn.ru/miph

Contents

Computer Science and Computer Engineering

Mathematical models in Physics

Discrete & Continuous Models
& Applied Computational Science
2020, 28 (2) 105–119
http://journals.rudn.ru/miph

Computer Science and Computer Engineering

Research article

UDC 519.872:519.217
DOI: 10.22363/2658-4670-2020-28-2-105-119

Comparative analysis of machine learning methods by the example of the problem of determining muon decay

Migran N. Gevorkyan[1], **Anastasia V. Demidova**[1], **Dmitry S. Kulyabov**[1,2]

[1] *Department of Applied Probability and Informatics*
Peoples' Friendship University of Russia (RUDN University)
6, Miklukho-Maklaya St., Moscow, 117198, Russian Federation

[2] *Laboratory of Information Technologies*
Joint Institute for Nuclear Research
6, Joliot-Curie St., Dubna, Moscow region, 141980, Russian Federation

(received: May 21, 2020; accepted: June 30, 2020)

The history of using machine learning algorithms to analyze statistical models is quite long. The development of computer technology has given these algorithms a new breath. Nowadays deep learning is mainstream and most popular area in machine learning. However, the authors believe that many researchers are trying to use deep learning methods beyond their applicability. This happens because of the widespread availability of software systems that implement deep learning algorithms, and the apparent simplicity of research. All this motivate the authors to compare deep learning algorithms and classical machine learning algorithms.

The Large Hadron Collider experiment is chosen for this task, because the authors are familiar with this scientific field, and also because the experiment data is open source. The article compares various machine learning algorithms in relation to the problem of recognizing the decay reaction $\tau^- \to \mu^- + \mu^- + \mu^+$ at the Large Hadron Collider. The authors use open source implementations of machine learning algorithms. We compare algorithms with each other based on calculated metrics. As a result of the research, we can conclude that all the considered machine learning methods are quite comparable with each other (taking into account the selected metrics), while different methods have different areas of applicability.

Key words and phrases: muon decay, machine learning, neural networks

1. Introduction

Machine learning is a branch of mathematical modeling related to the construction of surrogate statistics models. Recent years this area has been experiencing really intensive growth, related to the development of computer technology and the ability to analyze grate amount of data (Big Data). Nowadays machine learning approaches, in particular deep learning, demonstrate their high efficiency in data science. Particularly significant results are obtained in classification and cluster analysis of data with unknown structure. The most popular tendency in machine learning is deep learning. It became mainstream area in machine learning and other areas were pushed aside.

In this paper, the authors try to study if deep learning is really superior to all other machine learning methods. Previously, the authors conducted a comparative analysis of the most popular software products for working with neural networks networks [1], and also tried to generalize the methodology for working with machine learning models [2].

1.1. Paper structure

This paper has following structure. In section 2 we describe the problem of the decay reaction recognition $\tau^- \to \mu^- + \mu^- + \mu^+$. A brief introduction to the physics of the process is given.

The section 3 briefly describes the software we use.

The 4 section briefly describes the classification task, provides the terminology from the field of machine learning, we also consider metrics that are used to evaluate efficiency of classifiers.

We apply the Python language and the modules described to the problem in the section 3 . We use metrics to evaluate the effectiveness of various machine learning methods.

2. The violations of the Standard model

Currently, the main model that describes particle physics is a Standard model formulated in 1960–1970 [3]. Standard model it has passed many experimental tests. However, with from a methodological point of view, this theory is not satisfactory [4]. For example, the Standard model does not describe a number of phenomena, such as explanation of matter–antimatter asymmetry. Research in the field of theoretical and experimental physics that try to expand the standard model and describe phenomena that are not available to it have a collective name: physics beyond the standard model.

2.1. Preservation of lepton numbers

The Large Hadron Collider (LHC) is the main tool for studying physics beyond the Standard model. At the LHCb detector (LHG beauty experiment) experiments are being performed [5] whose purpose is the detection of phenomena that contradict theoretical settings of standard model. In particular, one of these phenomena is associated with violation of preserving the lepton

number (L) and the lepton flavor (L_e, L_μ, L_τ). For leptons, the heuristic division into three generations, which is necessary for existence asymmetries of matter and antimatter:

— the first generation consists of an electron and an electron neutrino (e^-, ν_e),
— second generation — muon and muon neutrino (μ^-, ν_μ),
— third generation — τ-lepton (tau) and tau neutrino (τ, ν_τ).

As we can see from the Table 1, according to the standard model each lepton has four numbers L_e, L_μ, L_τ and L and for every reactions between particles the sum of the numbers on the right side of the reaction equation must be equal to the sum of the numbers on the left side (Lepton number conservation).

Table 1

Reactions between particles in the standard model

Particle	e^-	e^+	μ^-	μ^+	τ^-	τ^+	ν_e	$\bar{\nu}_e$	ν_μ	$\bar{\nu}_\mu$	ν_τ	$\bar{\nu}_\tau$
L	+1	-1	+1	-1	+1	-1	+1	-1	+1	-1	+1	-1
L_e	+1	-1	0	0	0	0	+1	-1	0	0	0	0
L_μ	0	0	+1	-1	0	0	0	0	+1	-1	0	0
L_τ	0	0	0	0	+1	-1	0	0	0	0	+1	-1

This rule holds, for example, in the following tau decay reaction:

$$\tau^- \to e^- + \nu_\tau + \bar{\nu}_e,\ 1_\tau = 1_e + 1_\tau - 1_e.$$

However, there is a hypothetical tau decay reaction of the following type:

$$\tau^- \to \mu^- + \mu^- + \mu^+,\ 1_\tau \neq 1_\mu + 1_\mu - 1_\mu.$$

Ultrahigh energies proton collisions are performed at the LHC. On average the collision generates about 80 various particles, most of which are unstable and fast disintegrate. Among them, there are tau that can occur in one of the the next five reactions:

— Prompt $D_s^- \to \tau$,
— Prompt $D^- \to \tau$,
— Non-prompt $D_s^- \to \tau$,
— Non-prompt $D^- \to \tau$,
— $X_b \to \tau$.

The task is to build a classification model that must be trained to recognize the decay reaction $\tau^- \to \mu^- + \mu^- + \mu^+$. For training the classifier one [6] provides real data from LHC (background events) with the addition of signal data (signal events). The signal data is a simulation of the reaction $\tau^- \to \mu^-\mu^-\mu^+$.

The classifier requires the following two properties.

— Small discrepancy between real data and simulation. For Estimation of discrepancy data `check_agreement.csv` is provided This data relates to the reaction $D_s^+ \to \phi(\to \mu^-\mu^+)\pi^+$ which is topologically very similar to the desired response of the decay τ^-. Also the value of the Kolmogorov–Smirnov test coefficient must be less than 0.09.
— Also the classifier should have weak correlation with the mass τ^-. Data in a file is provided to evaluate the correlation `check_correlation.csv` and the Kramer–von Mises test (CvM).

3. Software

To apply all the described classification methods, we use Python language and a number of modules: SciKit Learn [7], Keras [8], `XGBoost` [9] and `hep_ml` [10]. Let's give a brief description here for each of them.

SciKit Learn [7] is library for data processing, which implements various methods of classification, regression analysis, clustering, and other algorithms related to machine learning training that does not use neural networks. The library is written in Python and uses a number of libraries from the SciPy stack to accelerate calculations. The current version has the number 0.22.2, but the project is quite mature.

SciKit Learn implements almost all of classifications algorithms we described. So the Logistic Regression method is implemented in a submodule `linear_model`, Gaussian Naive Bayes method is in the submodule `naive_bayes`, the `ensemble` submodule implements Random Forest and Gradient Boosting Classifier methods. In the submodule `sklearn.metrics` there are functions that calculate various metrics for estimation of quality of the classifier.

The XGBoost library is considered the best implementation of gradient boosting. It has API for many languages, including Python. We use it along with SciKit Learn to apply Gradient Boosting Classifier. Also due to the specifics of the task we use `hep_ml` module because it is specially designed for physics problems.

The Keras [8] library provides a high-level software interface for building neural networks. It can work on top of TensorFlow, Microsoft Cognitive Toolkit (CNTK) [11] or Theano [12]. The library is written completely in Python and distributed under the MIT license. Current version is 2.3.1. The library is based on the following principles: simplicity usage, modularity, and extensibility. Our choice of this libraries about is justified in the article [1].

The modularity principle allows one to describe neural layers separately, optimizers, activators, and so on, and then combine them into one model. The model is fully described in Python. Created model one can save to disk for future use and distribution.

4. Classification models

The classification model is based on an array of data, presented in tabular form. The process of model construction is usually consists of fitting numeric parameters and is also called *model training*. The propose of the model is to predict the value *dependent variable*. In the case of a binary classifier

a dependent variable can only take two values: 0 or 1. In in this case, the dependent variable is most often called *binary response* or just *response*. One can also meet the terms: goal, outcome, label, and Y–variable [13]–[15].

The model parameters are adjusted based on independent parameters variables that are represented by columns of the table. The following terms are also used: *predictor variable*, attribute and X–variable.

There are two types of predictor variables *numeric* and *factorial* (another term — *categorical*) predictor variables. Numeric variables are continuous and can take any values from some interval on the numeric axis, and the factor variables are discrete, not necessarily numeric, and can take values from a finite set. A special type of factor variables are *indicator* variables. Such variables accept only two values (0 or 1).

Depending on the model, it may be necessary to convert factor variables to numeric values or numeric to factor. So when applying multiple linear regression to an array of data with factor variables we need to convert them to numeric type. For example, we can use logit conversion. On the contrary, using the naive Bayesian classifier to continuous data, this data must be converted to factor type.

4.1. Metrics for evaluating classification models

A number of numerical methods are used to evaluate the classifier's performance characteristics (metrics) that allow us to compare different classifiers with each other and choose the most optimal one for the given tasks [14].

The classifier is evaluated based on *control* sample (also called *test* or *verification* sample). This sample consists of already classified elements and allows one to measure the performance of the classifier.

Let's assume that the size of the control sample is N and the binary classifier detects the response Y and assigns it 1 or 0. Since this detection is performed on the basis of a control sample, the event class is already known and we can check classification results. All possible predictions fit into four case.

1. True-positive (TP) — classification result is 1 and true value is 1;
2. False-negative (FN) — classification result is 0 but true value is 1;
3. False-positive (FP) — classification result is 1 but true value is 0;
4. True-negative (FN) — classification result is 0 and true value is 0.

Let's describe the main metrics that are used for classifier evaluation and specify functions from the module `sklearn.metrics` [7], [16], which are used to calculate this metrics.

Let the total sample size is N, and the classifier has defined TP true-positive, FN false-negative, FP false-positive and TN of true-negative cases. We can calculate the following table 2 called the *confusion matrix*.

The classification of metrics is based on this matrix. It shows the number of correct and incorrect predictions grouped into categories by response type. Other names of this matrix are error matrix or confusion matrix. To calculate this matrix we use the `confusion_matrix` function from SciKit–Learn library.

Accuracy is calculated as the percentage of events that the classifier identified correctly. Calculated using the formula:

$$Acc = \frac{TP + TN}{N},$$

Table 2

The confusion matrix

		Prediction		
		True (1)	False (0)	Total
Data	True (1)	TP	FN	$TP + FN$
	False (0)	FP	TN	$FP + TN$
	Total	$TP + FP$	$FN + TN$	N

and using the `accuracy_score` function.

Recall is the percentage of correctly classified events of type 1. Calculated using the formula:

$$R_{TP} = \frac{TP}{TP + FN},$$

and using the `recall_score` function. Terms are also used are *sensitivity* or true-positive rate.

Specificity is percentage of correctly classified events of type 0 (also called zeros). Calculated using the formula:

$$R_{FP} = \frac{TN}{TN + FN},$$

and also using the `recall_score` function (for binary classifier this function returns both recall and specificity). The term false-positive rate is also used.

Precision is percentage of predicted units that are actually zeros. Calculated using the formula:

$$Pcn = \frac{TP}{TP + FP},$$

and also using the `precision_score` function.

One can create a classifier that will relate all events to class 1. For such a classifier, the recall will be equal to 1, and specificity 0. An ideal classifier should detect events from class 1, without incorrectly identifying events of class 0, as events of the 1 class. Thus a balance must be maintained between recall and specificity. To evaluate this balance, one uses a graphical method called *ROC-curve* — receiver performance curve.

The ROC curve is a graph of recall versus specificity. For plotting on one axis is delayed recall, and on the other specificity. The graph of an absolutely ineffective classifier will be represent a diagonal line. More effective classifiers will have a graph in the form of an arc. The stronger the arc pressed against the upper-left corner, the more effective it is classifier. The data required to build the curve is calculated with the `roc_curve` function.

For a more accurate estimation of the ROC curve, one uses a metric indicator AUC — *area under the ROC curve*. A classifier with a ROC curve as a diagonal line will have $AUC = 0.5$. The more effective the classifier, the closer the AUC value is to 1. AUC is calculated by the `auc` function.

4.2. Logistic Regression

Logistic regression [17], [18] is an analog of multiple linear regression, with the exception of binary response. To adapt multiple linear regression for this case is necessary to do fallowing steps:

— represent the dependent variable as a probability function, with values from segment $[0, 1]$ (probabilistic outcome);
— apply the cutoff rule — any outcome with probability, greater than the threshold is classified as 1.

If classical multiple regression models the response as linear function from predictor variables:

$$y = \beta_0 + \beta_1 x_1 \beta_2 x_2 + \beta_3 x_3 + ... + \beta_n x_n,$$

then the logistics response function is modeled using the logistics response function (*logit-function* or *sigmoid*):

$$p = \frac{1}{1 + \exp(\beta_0 + \beta_1 x_1 \beta_2 x_2 + \beta_3 x_3 + ... + \beta_n x_n)}.$$

The range of values of such function is the interval $(0, 1)$, we can interpret its values as the probability of the response.

To fit parameters, we consider not the function itself, but the log-odds function:

$$l = \ln \frac{p}{1-p} = \beta_0 + \beta_1 x_1 \beta_2 x_2 + \beta_3 x_3 + ... + \beta_n x_n,$$

which map the probability p from the interval $(0, 1)$ to real numbers set. Then one uses the maximum likelihood method to select parameters based on a training sample.

After selecting the parameters it remains to select cut-off threshold. For example, if one puts it equal to 0.5, then all the response with value $p < 0.5$ will be classified as 0, and with the value $p >= 0.5$ as 1.

In the `sklearn` library, the function that implements the logistic regression algorithm is located in the `linear_model` module and it is called `LogisticRegression`.

4.3. Gaussian Naive Bayes

Naive Bayesian classifier [15], [19] is a binary classifier. Assignment to a particular class is based on the conditional probability $p(y|x_1, ..., x_n)$ which is calculated based on the Bayes theorem:

$$p(y|x_1, ..., x_n) = \frac{p(y, x_1, ..., x_n)}{p(x_1, ..., x_n)} = \frac{p(x_1, ..., x_n|y)p(y)}{p(x_1, ..., x_n)}.$$

Next, we make the «naive» statement that all predictor variables are independent and, therefore, the joint probability is $p(y, x_1, ..., x_n)$ and it can be calculated using the formula:

$$p(y, x_1, \dots, x_n) = p(y) \prod_{i=1}^{n} p(x_i|y).$$

If predictor variables are assumed to be numeric (i.e. continuous values), then a second «naive» statement is made about the continuity of the distribution function and about the type of distribution. Most often, the normal distribution and a Gaussian Naive Bayes classifier are used.

The advantages of a Naive Bayes classifier include simplicity (there are only few hyperparameter settings) and speed.

In the `sklearn` library, the function implementing the Gaussian Naive Bayes classifier algorithm is located in the `naive_bayes` module and is called `GaussianNB`.

4.4. Bagging and Random Forest

Tree models [20] or *decision trees* is a popular, relatively simple, and yet effective classification method.

Decision trees define a set of classification rules. The rules correspond to the sequential split of the data into segments. Each rule can be expressed as a «if-then» condition imposed on a predictor variable. For each predictor, *split value* is defined, which divides records into those where the value of the predictor variable is greater and those where it is less. A set of such rules forms a tree whose leaves correspond to one of the two required classes (for a binary classifier).

Tree models advantages is the simplicity of the results interpretation and the ability to reproduce the branching rules in natural language. However, one should avoid overtraining of these models. Overtraining means that branching rules start to take random noise into account. To prevent overtraining, one should limit the depth of tree branches.

Trees became particularly popular with the introduction of the *ensemble approach*. Its essence is to use a set of decision trees and train them on the same data with further taking the average or weighted average of their results.

Among the methods of training, a method called *bagging* or *bootstrap aggregation*. The bootstrap process involves repeatedly retrieving a random set of data from a sample. The number of extracted records is less than the sample size. The most common is bootstrap with replacement. Replacement means that the extracted data is returned to the sample after use, mixed, and used for subsequent retrievals. The begging process consists of training trees on multiple bootstrap samples with returns.

The *random forest* machine learning algorithm uses begging and selects predictor variables in addition to bootstrap. In other words, each new tree is built on a random subset of variables, rather than on all possible variables. There is empirical rule that it is most efficient to select only $\sqrt{n}$ predictor variables from n each time.

In the `sklearn` library, the function that implements the random forest algorithm is located in the `ensemble` module and is called `RandomForestClassifier`.

4.5. Gradient Boosting Classifier

Gradient boosting method [21] consists of combining a large number of simple models to produce one that is more accurate than each individual simple model itself. A set of simple models is called *ensemble*, and by boosting we mean the sequential process of building simple models.

The gradient boosting algorithm is one of the most commonly used machine learning algorithms. We will give only a brief qualitative description here, without going into mathematical details [22], [23].

At each step of gradient boosting, the selected loss function is minimized by gradient descent. The loss function is constructed for the selected base algorithm. Most often the underlying algorithm is the decision tree algorithm. When building each subsequent model, the errors of the previous one are taken into account. This is done by defining the data that does not fit into the previous simple model and adding the next model that processes this data correctly. When configuring the algorithm, the maximum number of models in the ensemble is specified, and when this number of iterations is reached, the algorithm stops. Each model from the ensemble is assigned a certain weight and their predictions are generalized.

In the `sklearn` library, the function that implements the gradient boosting algorithm is located in the `ensemble` module and is called `GradientBoostingClassifier`.

In addition to the implementation included in `scikitlearn`, Python also has the `XGBoost` [9] library, which is highly optimized and has interfaces for a large number of programming languages (C/C++, Java, Ruby, Julia, R).

In addition to the implementations from these two libraries, we used the gradient boosting implementation from the `hep_ml` [10] library, which contains machine learning methods used in the field of high-energy physics.

4.6. Neural Network

In the article [1], the authors compared various libraries for building neural networks [8], [12], [24]–[26]. The result of the speed and the accuracy tests show that Keras library provides the most optimal solution. Therefore, to solve the problem of recognizing the decay reaction $\tau^- \to \mu^- + \mu^- + \mu^+$ we build neural network using this library.

5. Application of the considered methods

We carry out a comparative analysis of classifiers from section 4 by applying them to the problem of determining muon decay. The problem is a binary classification problem and is based on data from the LCH and generated data for detecting muon decay. Training and test data are presented in csv files. The data contains the values of 40 analyzed parameters. The target attribute is the «signal» attribute, which takes the values 0 or 1. For training classifiers, the data set was divided into training and test samples in the ratio of 8 to 2, the number of records for training classifiers is 54042, and the number of records for testing is 13511.

We choose MLP (multi-layer perceptron) architecture for the neural network. The network consists of fully connected layers with Batch Normalization layers

between them that prevent overtraining. Each of the fully connected layers contains a different number of neurons. The input layer consists of 28 neurons, the hidden layers contain 100, 120, 60, and 20 neurons, and the output layer contains 2, according to the number of classes in the data.

All classifiers were tested on a small discrepancy between real data and simulation (Kolmogorov–Smirnov test, the test value for the classifier should be less than 0.09) and a weak correlation with ground test (Cramer–von Mises (CvM), the test value for the classifier should be less than 0.002) In the table 3 lists the values of these tests.

Table 3

Results of the Kolmogorov–Smirnov and the Kramer–von Mises tests

Classification	Kolmogorov–Smirnov test	Kramer–von Mises test
Random Forest	0.03682	0.00092
Logistic Regression	0.03309	0.00103
Gaussian Naive Bayes	0.04722	0.00113
Gradient Boosting Classifier	0.05162	0.00089
Xgboost	0.06327	0.00089
UGradient Boosting Classifier	0.05587	0.00102
MLP	0.01139	0.00079

For all classifiers, the main metrics are calculated (table 4) for test data, and the results of comparing the classifiers are presented as a diagram (Figure 1).

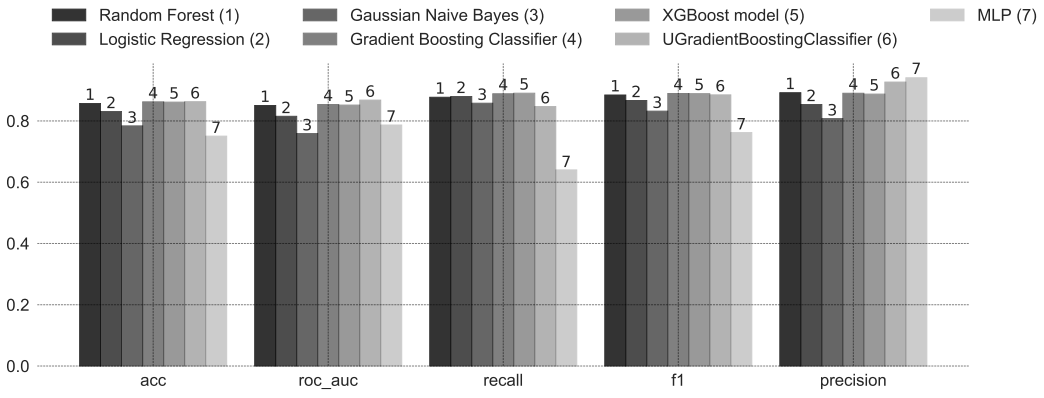

Figure 1. The results of the comparative analysis of classifiers

Table 4

The metric values on the test data

Classification	Accuracy	ROC-AUC	Recall	F1	Rrecision
Random Forest	0.857	0.851	0.877	0.885	0.892
Logistic Regression	0.831	0.815	0.880	0.867	0.854
Gaussian Naive Bayes	0.784	0.759	0.858	0.832	0.808
Gradient Boosting Classifier	0.862	0.854	0.889	0.889	0.890
xgboost	0.861	0.853	0.890	0.889	0.888
UGradient-BoostingClassifier	0.863	0.868	0.847	0.885	0.927
MLP	0.750	0.787	0.640	0.762	0.941

6. Discussion

The paper presents a comparative analysis of various machine learning algorithms on the example of the problem of determining the decay reaction $\tau^- \to \mu^- + \mu^- + \mu^+$ at the LHC. We study following algorithms: Logistic Regression, Gaussian naive Bayes classifier, gradient boosting classifier, bootstrap aggregating (bagging) and random forest, neural network model (machine learning algorithm — MLA). For each of the algorithms, we build a classifier using Python libraries and calculate metrics calculated that can be used to determine the most effective model.

All classifiers successfully passed tests for a small discrepancy between real data and simulation (Kolmogorov–Smirnov test) and for a weak correlation with mass (Kramer–von Mises test), which indicates a good quality of the constructed classifiers for this problem.

To conduct a comparative analysis of machine learning methods, we calculate the most important metrics for each model: accuracy, ROC–AUC score, recall, F1-score, precision. In the aggregate of all metrics, the random forest and the gradient boosting method (and their modifications) have the best results. Logistic Regression, Gaussian Naive Bayes and a model based on a fully connected neural network show worse results. However, the neural network surpass other classifiers by the value of the precision metric. This means that the neural network can better distinguish classes from each other than other classifiers.

7. Conclusion

A comparative analysis of various machine learning algorithms is carried out on the example of the problem of determining the decay reaction $\tau^- \to \mu^- + \mu^- + \mu^+$ at the Large Hadron Collider. As the compared algorithms were chosen: Logistic Regression, Naive Bayesian approach with normal distribution, the method of gradient boosting (Gradient boosting classifier), bootstrap aggregation in combination with random forest, a model based on a neural network (machine learning algorithm—MLA). For each of the algorithms, using the libraries for the Python language, a classifier was built and metrics were calculated, based on which the most effective model can be determined.

Acknowledgments

The publication has been prepared with the support of the Russian Foundation for Basic Research (RFBR) according to the research project No 19-01-00645.

References

[1] M. N. Gevorkyan, A. V. Demidova, T. S. Demidova, and A. A. Sobolev, "Review and comparative analysis of machine learning libraries for machine learning," *Discrete and Continuous Models and Applied Computational Science*, vol. 27, no. 4, pp. 305–315, Dec. 2019. DOI: 10.22363/2658-4670-2019-27-4-305-315.

[2] L. A. Sevastianov, A. L. Sevastianov, E. A. Ayrjan, A. V. Korolkova, D. S. Kulyabov, and I. Pokorny, "Structural Approach to the Deep Learning Method," in *Proceedings of the 27th Symposium on Nuclear Electronics and Computing (NEC-2019)*, V. Korenkov, T. Strizh, A. Nechaevskiy, and T. Zaikina, Eds., ser. CEUR Workshop Proceedings, vol. 2507, Budva, Sep. 2019, pp. 272–275.

[3] P. Langacker, *The standard model and beyond*, ser. Series in High Energy Physics, Cosmology and Gravitation. CRC Press, 2009.

[4] I. Lakatos, "Falsification and the Methodology of Scientific Research Programmes," in *Criticism and the growth of Knowledge*, I. Lakatos and A. Musgrave, Eds., Cambr. University Press, 1970, pp. 91–195.

[5] R. Aaij *et al.*, "Search for the lepton flavour violating decay $\tau - \to \mu - \mu + \mu -$," *Journal of High Energy Physics*, vol. 2015, no. 2, p. 121, Feb. 2015. DOI: 10.1007/JHEP02(2015)121. arXiv: 1409.8548.

[6] (2018). "Flavours of Physics: Finding $\tau \to \mu\mu\mu$ (Kernels Only)," [Online]. Available: https://www.kaggle.com/c/flavours-of-physics-kernels-only.

[7] F. Pedregosa *et al.*, "Scikit-learn: Machine Learning in Python," *Journal of Machine Learning Research*, vol. 12, pp. 2825–2830, 2011.

[8] F. Chollet. (2020). "Keras," [Online]. Available: https://keras.io/.

[9] (2020). "XGBoost Documentation," [Online]. Available: https://xgboost.readthedocs.io.

[10] (2020). "Hep_ml," [Online]. Available: https://arogozhnikov.github.io.

[11] (2020). "CNTC official repository," [Online]. Available: https://github.com/Microsoft/cntk.

[12] Theano Development Team, "Theano: A Python framework for fast computation of mathematical expressions," *arXiv e-prints*, vol. abs/1605.0, 2016.

[13] I. H. Witten, E. Frank, M. A. Hall, and C. J. Pal, *Data Mining: Practical Machine Learning Tools and Techniques*, ser. The Morgan Kaufmann Series in Data Management Systems. Elsevier, 2011. DOI: 10.1016/C2009-0-19715-5.

[14] A. Bruce and P. Bruce, *Practical Statistics for Data Scientists: 50 Essential Concepts*. O'Reilly Media, 2017.

[15] J. VanderPlas, *Python Data Science Handbook: Essential Tools for Working with Data*. O'Reilly Media, 2016.

[16] (2020). "Scikit-learn home site," [Online]. Available: https://scikit-learn.org/stable/.

[17] D. W. Hosmer, S. Lemeshow, and R. X. Sturdivant, *Applied Logistic Regression*, ser. Wiley Series in Probability and Statistics. Wiley, 2013.

[18] J. M. Hilbe, *Logistic Regression Models*, ser. Chapman & Hall/CRC Texts in Statistical Science. Chapman and Hall/CRC, May 2009. DOI: 10.1201/9781420075779.

[19] D. Ruppert, "The Elements of Statistical Learning: Data Mining, Inference, and Prediction," *Journal of the American Statistical Association*, Springer Series in Statistics, vol. 99, no. 466, p. 567, 2004. DOI: 10.1198/jasa.2004.s339.

[20] R. Collins, *Machine Learning with Bagging and Boosting*. Amazon Digital Services LLC - Kdp Print Us, 2018.

[21] J. H. Friedman, "Greedy function approximation: A gradient boosting machine," *Annals of Statistics*, vol. 29, no. 5, pp. 1189–1232, 2001. DOI: 10.2307/2699986.

[22] A. W. Kemp and B. F. J. Manly, *Randomization, Bootstrap and Monte Carlo Methods in Biology*. Ser. Chapman & Hall/CRC Texts in Statistical Science 4. CRC Press, Dec. 1997, vol. 53. DOI: 10.2307/2533527.

[23] O. Soranson, *Python Data Science Handbook: The Ultimate Guide to Learn How to Use Python for Data Analysis and Data Science. Learn the Essential Tools for Beginners to Work with Data*, ser. Artificial Intelligence Series. Amazon Digital Services LLC - KDP Print US, 2019.

[24] M. Abadi, A. Agarwal, Paul Barham, EugeneBrevdo, Zhifeng Chen, Craig Citro, Greg S. Corrado, Andy Davis, and Jeffrey Dean. (2015). "TensorFlow: Large-Scale Machine Learning on Heterogeneous Systems," [Online]. Available: http://tensorflow.org/.

[25] (2020). "TensorFlow home site," [Online]. Available: https://www.tensorflow.org/.

[26] A. Paszke, S. Gross, S. Chintala, G. Chanan, E. Yang, Z. DeVito, Z. Lin, A. Desmaison, L. Antiga, and A. Lerer, "Automatic differentiation in PyTorch," in *31st Conference on Neural Information Processing Systems (NIPS 2017), Long Beach, CA, USA*, 2017.

For citation:

M. N. Gevorkyan, A. V. Demidova, D. S. Kulyabov, Comparative analysis of machine learning methods by the example of the problem of determining muon decay, Discrete and Continuous Models and Applied Computational Science 28 (2) (2020) 105–119. DOI: 10.22363/2658-4670-2020-28-2-105-119.

Information about the authors:

Migran N. Gevorkyan (Russian Federation) — Candidate of Sciences in Physics and Mathematics, Assistant Professor of Department of Applied Probability and Informatics of Peoples' Friendship University of Russia (RUDN University) (e-mail: gevorkyan-mn@rudn.ru, phone: +7(495)9550927, ORCID: https://orcid.org/0000-0002-4834-4895, ResearcherID: E-9214-2016, Scopus Author ID: 57190004380)

Anastasia V. Demidova (Russian Federation) — Candidate of Sciences in Physics and Mathematics, Assistant Professor of Department of Applied Probability and Informatics of Peoples' Friendship University of Russia (RUDN University) (e-mail: demidova-av@rudn.ru, phone: +7(495)9550927, ORCID: https://orcid.org/0000-0003-1000-9650, ResearcherID: AAD-2214-2019, Scopus Author ID: 57191952809)

Dmitry S. Kulyabov (Russian Federation) — Docent, Doctor of Sciences in Physics and Mathematics, Professor at the Department of Applied Probability and Informatics of Peoples' Friendship University of Russia (RUDN University) (e-mail: kulyabov-ds@rudn.ru, phone: +7 (495) 952-02-50, ORCID: https://orcid.org/0000-0002-0877-7063, ResearcherID: I-3183-2013, Scopus Author ID: 35194130800)

УДК 519.872:519.217
DOI: 10.22363/2658-4670-2020-28-2-105-119

Сравнительный анализ методов машинного обучения на примере задачи определения мюонного распада

М. Н. Геворкян[1], **А. В. Демидова**[1], **Д. С. Кулябов**[1, 2]

[1] *Кафедра прикладной информатики и теории вероятностей*
Российский университет дружбы народов
ул. Миклухо-Маклая, д. 6, Москва, 117198, Россия
[2] *Лаборатория информационных технологий*
Объединённый институт ядерных исследований
ул. Жолио-Кюри, д. 6, Дубна, Московская область, 141980, Россия

Применение алгоритмов машинного обучения для анализа статистических моделей имеет достаточно длинную историю. Развитие компьютерной техники дало этим алгоритмам новое дыхание. Особенно громкую известность получило такое направление машинного обучения, как глубинное обучение. Однако авторы полагают, что многие исследователи пытаются использовать методы глубинного обучения за пределами их применимости. Этому способствуют как широкая распространённость программных комплексов, реализующих алгоритмы глубинного обучения, так и кажущаяся простота исследования. Всё это стало побудительным мотивом для проведения сравнения алгоритмов глубинного обучения и классических алгоритмов машинного обучения.

В качестве задачи был выбран эксперимент на Большом адронном коллайдере, поскольку авторы знакомы с данной научной областью, а также потому, что данные эксперимента доступны публично. В статье проводится сравнение различных алгоритмов машинного обучения применительно к задаче распознания реакции распада $\tau^- \to \mu^- + \mu^- + \mu^+$ на Большом адронном коллайдере. Используются готовые свободные реализации алгоритмов машинного обучения. Алгоритмы сравниваются друг с другом на основе вычисляемых метрик. В результате исследования можно сделать вывод, что все рассмотренные методы машинного обучения вполне сопоставимы друг с другом (с учётом выбранных метрик), при этом разные методы имеют разные области применимости.

Ключевые слова: мюонный распад, машинное обучение, нейронные сети

Mathematical models in Physics

Research article

UDC 524.834
PACS 07.05.Tp, 98.80.Es,
DOI: 10.22363/2658-4670-2020-28-2-120-130

Applying Friedmann models to describe the evolution of the Universe based on data from the SAI Supernovae Catalog

Arsenii S. Gavrikov[1], **Bijan Saha**[1, 2], **Victor S. Rikhvitsky**[2]

[1] *Institute of Physical Research and Technology*
Peoples' Friendship University of Russia (RUDN University)
6, Miklukho-Maklaya St., Moscow, 117198, Russian Federation
[2] *Laboratory of Information Technologies*
Joint Institute for Nuclear Research
6, Joliot-Curie St., Dubna, Moscow region, 141980, Russian Federation

(received: April 18, 2020; accepted: June 30, 2020)

In the recent years thanks to the modern and sophisticated technologies the astronomers and astrophysicists were able to look deep into the Universe. This vast data poses some new problem to the cosmologists. One of the problems is to develop an adequate theory. Another one is to fit the theoretical results with the observational one. In this report within the scope of the isotropic and homogeneous Friedman–Lemaitre–Robertson–Walker (FLRW) cosmological model we study the evolution of the Universe filled with dust or cosmological constant. The reason to consider this model is the present universe surprisingly homogeneous and isotropic in large scale. We also compare our results with the data from the SAI Supernovae Catalog. Since the observational data are given in terms of Hubble constant (H) and redshift (z) we rewrite the corresponding equations as a functions of z. The task is to find the set of parameters for the mathematical model of an isotropic and homogeneous Universe that fits best with the astronomical data obtained from the study of supernovae: magnitude (m), redshift (z).

Key words and phrases: fitting, cosmology, Friedmann's Universe, data analysis

1. Introduction

Based on modern data, it is established that the universe is not stationary today, but it is expanding with acceleration [1]–[8]. This fact was established by studying large amounts of data on supernovae, including those that are remote in huge distances. The peculiarity of this work is that the objects

contained in the database [9], [10] are located mainly at distances of non-cosmological scale, which may be reflected in the descriptive power of certain Friedmann models of the Universe.

2. Friedmann model

The equations of General relativity describing the evolution of the Universe are complex enough to solve them exactly. So Friedmann suggested that we instead accept two simple assumptions: (1) the universe looks exactly the same in all directions; (2) this condition holds true for all its points. Based on General relativity and these two simple assumptions, Friedmann showed [11] that the universe may not be stationary. This model was further independently developed by Lemaitre [12], Robertson [13]–[15] and Walker [16].

The equations describing the evolution of the Universe, and which we will solve, look like this:

$$\begin{cases} \dot{H} + H^2 = -\dfrac{4\pi G}{3}(\varepsilon + 3p), \\ \dot{a} = Ha, \\ \dot{\varepsilon} = -3H(\varepsilon + p). \end{cases} \tag{1}$$

Here: H — Hubble parameter, a — scale factor, ε — energy density, p — pressure. To solve this system, we need another condition — the connection between p and ε.

Let $p = f(\varepsilon)$. This relationship is called the equation of state. In our case (the dust Universe), this equation reduces to a trivial one: $p = 0$.

Let's go back to system (1), which is a system of differential equations with respect to time. First, we need to go from time to redshift, since the observational data contains this value.

The red-shift is defined as

$$z = \frac{\lambda_o - \lambda}{\lambda}, \tag{2}$$

here λ_o is the wavelength during detection, λ is the wavelength during emission.

$$1 + z = \frac{\lambda_o}{\lambda} = \frac{\nu_o}{\nu} = \frac{a(t_o)}{a(t)}, \tag{3}$$

$$\frac{dz}{dt} = -\frac{a(t_o)}{a^2(t)}\dot{a}(t) = -\frac{a(t_o)}{a(t)}\frac{\dot{a}(t)}{a(t)} = -(z+1)H. \tag{4}$$

Using equations (4), (3), and the second equation from the system (1), we obtain the first equation for the scale factor with respect to z:

$$\frac{da}{dz} = -\frac{a(t_o)}{(z+1)^2}. \tag{5}$$

Similarly for the equation on H:

$$\frac{dH}{dz}\frac{dz}{dt} + H^2 = -\frac{4\pi G}{3}(\varepsilon + 3p) => \frac{dH}{dz} = \frac{1}{1+z}\left[H + \frac{4\pi G}{3H}(\varepsilon + 3p)\right]. \quad (6)$$

The third equation from system (1) is converted to an equation with respect to a. Then the result (1) is rewritten as:

$$\begin{cases} \dfrac{dH}{dz} = \dfrac{1}{1+z}\left[H + \dfrac{4\pi G}{3H}(\varepsilon + 3p)\right], \\ \dfrac{da}{dz} = -\dfrac{a(t_o)}{(z+1)^2}, \\ \dfrac{d\varepsilon}{\varepsilon + p} = -3\dfrac{da}{a}. \end{cases} \quad (7)$$

Since the astronomical data contains a magnitude, it is necessary to associate the Hubble parameter with the magnitude. Let's do this with another equation — the equation for the distance that light travels:

$$\frac{dD}{dt} = c => \frac{dD}{dz}\frac{dz}{dt} = c => \frac{dD}{dz} = -\frac{c}{(1+z)H}, \quad (8)$$

and the equation for magnitude:

$$m = -2.5 \lg \frac{D_0^2}{D^2}, \quad (9)$$

The complete system of equations will then take the form:

$$\begin{cases} \dfrac{dH}{dz} = \dfrac{1}{1+z}\left[H + \dfrac{4\pi G}{3H}(\varepsilon + 3p)\right], \\ \dfrac{da}{dz} = -\dfrac{a(t_o)}{(z+1)^2}, \\ \dfrac{d\varepsilon}{\varepsilon + p} = -3\dfrac{da}{a}, \\ \dfrac{dD}{dz} = -\dfrac{c}{(1+z)H}, \\ m = -2.5 \lg \dfrac{D_0^2}{D^2}. \end{cases} \quad (10)$$

With the condition $p = 0$:

$$\varepsilon = \varepsilon_o (1+z)^3. \quad (11)$$

Substitute (11) and $p = 0$ in the first equation from (10), then the solution of this dif. equations with the initial condition $H(0) = H_0$:

$$H = \sqrt{\frac{8\pi G\varepsilon_0}{3}(1+z)^3 + \left(H_0^2 - \frac{8\pi G\varepsilon_0}{3}\right)(1+z)^2}. \tag{12}$$

Substitute (12) in the fourth equation from (10):

$$\alpha = H_0^2 - \frac{8\pi G\varepsilon_0}{3}, \quad \beta = \frac{8\pi G\varepsilon_0}{3}.$$

$$D = -c\int \frac{dz}{(1+z)^2[\alpha+\beta(z+1)]^{\frac{1}{2}}}. \tag{13}$$

Substituting $\beta x + \alpha = t^2$ and integrating with the condition $D(0) = 0$, we get:

$$D = -\frac{\beta}{\alpha^{\frac{3}{2}}}\ln\frac{\sqrt{\alpha}+\sqrt{\alpha+\beta(1+z)}}{\sqrt{1+z}(\sqrt{\alpha}+\sqrt{\alpha+\beta})} - \\ - \frac{\sqrt{\alpha+\beta}(1+z) - \sqrt{\alpha+\beta(1+z)}}{\alpha(1+z)}. \tag{14}$$

The results of the approximation are shown in the table 1.

Table 1

The result of the approximation in the case of $w = 0$ (dust)

RMSE	MSE	H_0, (km/s)/Mpc	Ω_m	D_0, m
1.4438	1.0478	68.0001	5.7764	9.7200×10^{20}

In the third equation from (10) we get rid of time and substitute $p = 0$, we get:

$$\varepsilon = \varepsilon_0 a^{-3}. \tag{15}$$

Now substitute H from the second equation from (1) and (15) to the first equation from (1):

$$\ddot{a} = -\frac{4\pi G}{3}\varepsilon_0 a^{-2}. \tag{16}$$

We also solve it numerically with initial conditions $a(0) = 1$, $\dot{a}(0) = H_0$.

3. LCDM-model

LCDM-model is short for Lambda-Cold Dark Matter, a modern cosmological model based on the assumption of isotropy and homogeneity of the Universe [17]. The space environment in this model consists of several components: dark energy (Λ-member), cold dark matter, ordinary matter, and radiation.

Table 2

LCMD-model parameters

H_0, (km/s)/Mpc	Ω_m	Ω_{rad}	ε_{crit}, kg/m^3	Ω_Λ
67.74	0.3082	0.0001	8.62×10^{-27}	0.6911

Model parameters [18] are shown in table 2.
The first and fourth equations from (10) will take the form:

$$\begin{cases} \dfrac{dH}{dz} = \dfrac{H}{1+z} + \dfrac{H_0^2}{H}\left(\Omega_{rad}(1+z)^3 + \dfrac{1}{2}\Omega_m(1+z)^2 - \Omega_\Lambda(1+z)^{-1}\right), \\ \dfrac{dD}{dz} = -\dfrac{c}{(1+z)H}. \end{cases} \tag{17}$$

And equation for the scale factor:

$$\ddot{a} = -H_0^2\left(\Omega_{rad}a^{-3} + \frac{1}{2}\Omega_m a^{-2} - \Omega_L a\right). \tag{18}$$

We also solve it numerically with initial conditions $\dot{a}(0) = H_0$, $a(0) = 1$. RMSE and MSE for the LCDM model are 1.4612 and 1.0579, respectively.

4. Comparison of models

Comparison of theoretical results and observations within the scope of LRS Bianchi type-I model was performed in [19]–[21].

An approximation of the m(z) curve using the parameters of the LCDM model and the Friedmann model is shown in figure 1.

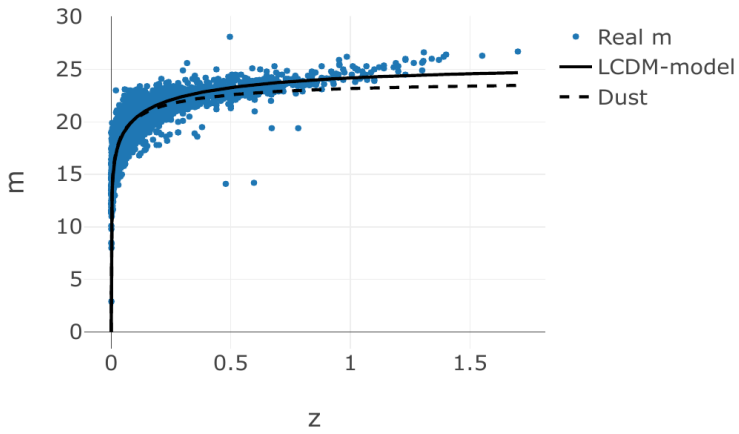

Figure 1. The dependence of the magnitude on the redshift for the LCDM-model and the Friedmann model

The dependencies of $H(z)$ are shown in figure 2, and the dependencies of the scale factor and Hubble parameter on time are shown in figures 3–5.

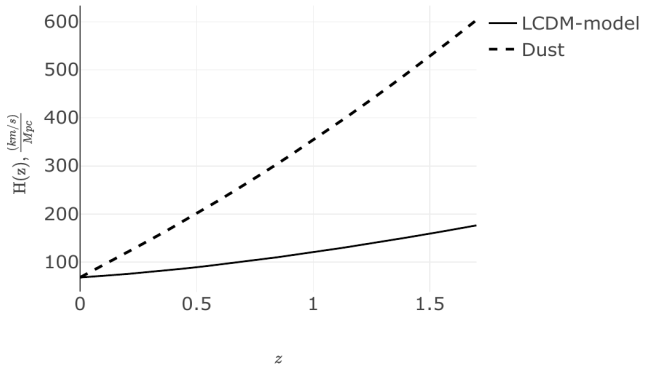

Figure 2. Dependence of the Hubble parameter on the redshift for the LCDM-model and the Friedmann model

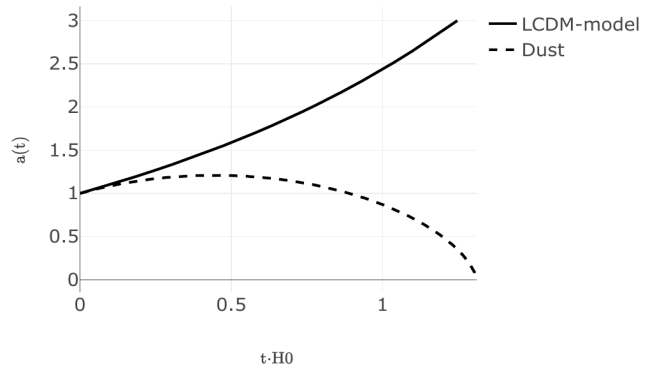

Figure 3. Dependence of the scale factor on time for the LCDM-model and the Friedmann model

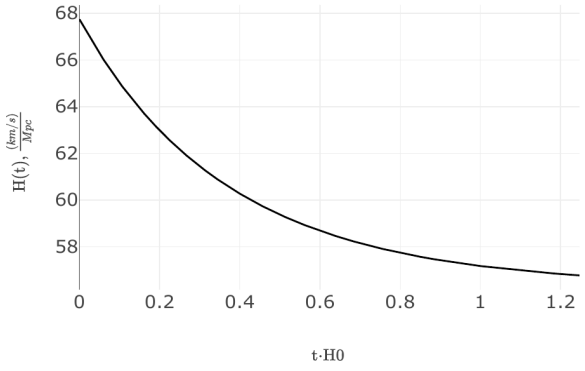

Figure 4. Dependence of the Hubble parameter on time for the LCDM-model

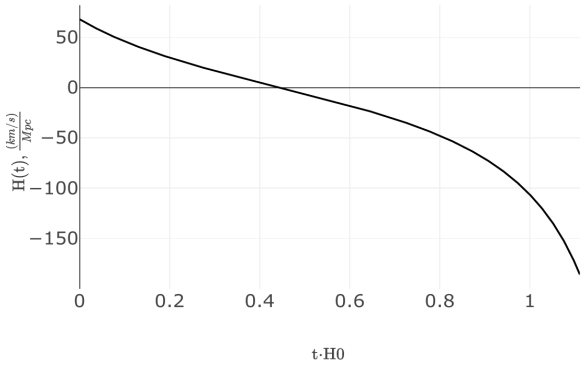

Figure 5. Dependence of the Hubble parameter on time for the Friedmann model

Table 3

Metrics for the quality of models for all z

RMSE	MSE	Model
1.4438	1.0478	Dust
1.4612	1.0579	LCDM

Comparison of quality metrics is shown in table 3.

Thus, it can be seen that the data from the SAI Supernovae Catalog is better described by the model of the dust Universe with a critical density of $\Omega_m = 5.7764$ than by the LCDM model. The Friedmann universe collapses after $\approx 1.3t_0$ of the age of the Universe ($t_0 = 1/H_0$). In turn, the LCDM model simulates an expanding Universe with acceleration. The explanation for this conclusion is the fact that the data contains a huge number (5359 out of 5614) of supernovae located in regions where the redshift $z < 0.5$. At scales where $z < 0.5$, the model of the Friedmann Universe is more efficient.

Let's look at this in more detail. Divide our data into two sets: the first data set will contain data with redshift values $z < 0.5$, and the second data set with redshift values $z > 0.5$.

We get approximations in these cases. The results are shown in figures 6–7.

Quality metrics in tables 4–5.

Table 4

Metrics for the quality of models at $z < 0.5$

RMSE	MSE	Model
1.4502	1.0506	Dust
1.4803	1.0781	LCDM

Table 5

Metrics for the quality of models at $z > 0.5$

RMSE	MSE	Model
1.0888	0.7285	Dust
0.9602	0.6001	LCDM

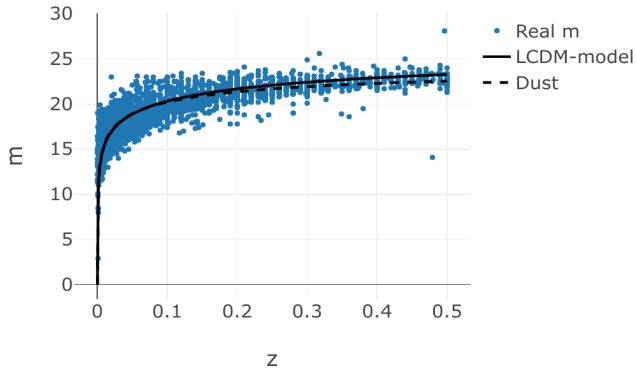

Figure 6. The dependence of the magnitude on the redshift for the LCDM-model and the Friedmann model at $z < 0.5$

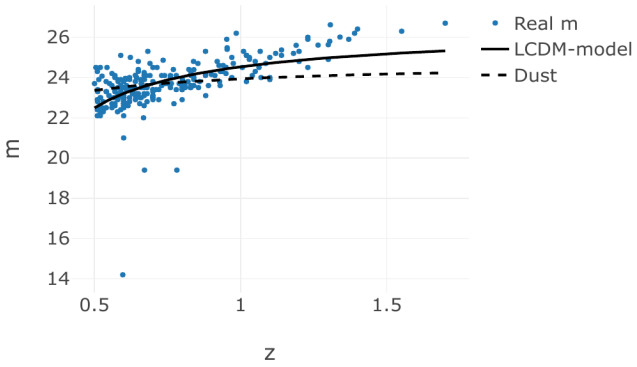

Figure 7. The dependence of the magnitude on the redshift for the LCDM-model and the Friedmann model at $z > 0.5$

5. Discussion

As we have already mentioned, thanks to modern technology astronomers and astrophysicists have been gathering a huge number of data about the past and present of our Universe. These helps us not only understand the past of the Universe, but also predict the future. Based on those data cosmologists try to construct the theoretical models and compare them with the observational data obtain the reliable one. Here we did the same within the scope of the simplest models. The idea was to construct some mathematical models which can be used in future for more complicated and realistic cases.

6. Conclusions

It was shown that the efficiency of the LCDM-model based on dark energy dominance better describes the behavior of the Universe at large scales than the model based on dust dominance. This corresponds to the modern view of the evolution of the Universe.

Acknowledgments

The publication has been prepared with the support of the "RUDN University Program 5-100" and funded by RFBR according to the research projects No. 18-07-00692 and No. 16-07-00766.

References

[1] A. Riess, A. Filippenko, Challis, and et al., "Observational Evidence from Supernovae for an Accelerating Universe and a Cosmological Constant," *The Astronomical Journal*, vol. 116, p. 1009, 1998. DOI: 10.1086/300499.

[2] A. G. Riess, L.-G. Strolger, J. Tonry, S. Casertano, and et al., "Type Ia Supernova Discoveries at z $>$ 1 from the Hubble Space Telescope: Evidence for Past Deceleration and Constraints on Dark Energy Evolution," *The Astrophysical Journal*, vol. 607, no. 2, pp. 665–687, Jun. 2004. DOI: 10.1086/383612.

[3] S. Perlmutter, G. Aldering, G. Goldhaber, and et al., "Measurements of Ω and Λ from 42 High-Redshift Supernovae," *The Astrophysical Journal*, vol. 517, no. 2, pp. 565–586, Jun. 1999. DOI: 10.1086/307221.

[4] S. Perlmutter and et al., "Discovery of a supernova explosion at half the age of the Universe," *Nature*, vol. 391, pp. 51–54, 1998. DOI: 10.1038/34124.

[5] C. L. Bennett *et al.*, "First-Year Wilkinson Microwave Anisotropy Probe (WMAP) Observations: Preliminary Maps and Basic Results," *The Astrophysical Journal Supplement Series*, vol. 148, no. 1, pp. 1–27, Sep. 2003. DOI: 10.1086/377253.

[6] B. Saha, "Nonlinear spinor field in Bianchi type-I cosmology: Inflation, isotropization, and late time acceleration," *Phys. Rev. D*, vol. 74, Dec. 2006. DOI: 10.1103/PhysRevD.74.124030.

[7] A. Pradhan and B. Saha, "Accelerating dark energy models of the universe in anisotropic Bianchi type space-times and recent observations," *Physics of Particles and Nuclei*, vol. 46, Mar. 2015. DOI: 10.1134/S1063779615030028.

[8] B. Saha, "Spinor Field Nonlinearity and Space-Time Geometry," *Physics of Particles and Nuclei*, vol. 49, pp. 146–212, Mar. 2018. DOI: 10.1134/S1063779618020065.

[9] O. Bartunov, D. Tsvetkov, and N. Pavlyuk, "Sternberg Astronomical Institute Supernova Catalogue, and Radial Distribution of Supernovae in Host Galaxies," in *Proceedings of the International Astronomical Union*, vol. 2, Aug. 2006, pp. 316–316. DOI: 10.1017/S1743921307010812.

[10] O. Bartunov, D. Tsvetkov, and N. Pavlyuk, "SAI Supernova Catalog," Accessed: 2020-03-01.

[11] A. Friedman, "Über die Krümmung des Raumes," *Z. Phys.*, vol. 10, pp. 377–386, Dec. 1922. DOI: 10.1007/BF01332580.

[12] G. Lemaître, "L'Univers en expansion," *Annales de la Societe Scietifique de Bruxelles*, vol. 53, p. 51, Jan. 1933.

[13] H. Robertson, "Kinematics and World-Structure," *The Astrophysical Journal*, vol. 82, p. 284, Oct. 1935. DOI: 10.1086/143681.

[14] H. Robertson, "Kinematics and World-Structure II.," *The Astrophysical Journal*, vol. 83, p. 187, Apr. 1936. DOI: 10.1086/143716.

[15] H. Robertson, "Kinematics and World-Structure III.," *The Astrophysical Journal*, vol. 83, p. 257, May 1936. DOI: 10.1086/143726.

[16] A. G. Walker, "On Milne's Theory of World-Structure," *Proceedings of the London Mathematical Society*, vol. 42, pp. 90–127, Jan. 1937.

[17] A. Liddle, *An Introduction to Modern Cosmology (2nd ed.)* Wiley, 2003, 189 pp.

[18] P. Ade, "Planck 2015 results. XIII. Cosmological parameters," *Astronomy & Astrophysics*, vol. 594, Oct. 2016. DOI: 10.1051/0004-6361/201525830.

[19] B. Saha and V. S. Rikhvitsky, "Nonlinear spinor fields in LRS Bianchi type-I space-time: Theory and observation," *Gravitation and Cosmology*, vol. 23, no. 4, pp. 329–336, Oct. 2017. DOI: 10.1134/s0202289317040193.

[20] M. O. Farooq, D. Mania, and B. Ratra, "Observational constraints on non-flat dynamical dark energy cosmological models," *Astrophysics and Space Science*, vol. 357, Aug. 2013. DOI: 10.1007/s10509-015-2319-2.

[21] M. O. Farooq, "Observational constraints on dark energy cosmological model parameters," Sep. 2013. arXiv: 1309.3710.

For citation:
A. S. Gavrikov, B. Saha, V. S. Rikhvitsky, Applying Friedmann models to describe the evolution of the Universe based on data from the SAI Supernovae Catalog, Discrete and Continuous Models and Applied Computational Science 28 (2) (2020) 120–130. DOI: 10.22363/2658-4670-2020-28-2-120-130.

Information about the authors:
Gavrikov, Arsenii S. — Student of the Institute of Physical Research and Technologies, Peoples' Friendship University of Russia (RUDN University) (e-mail: gavrikov.997755@gmail.com, phone: +7(999)7198668, ORCID: https://orcid.org/0000-0002-6741-5409)

Saha, Bijan — Doctor of Physical and Mathematical Sciences, assistant professor of the Institute of Physical Research and Technologies of Peoples' Friendship University of Russia (RUDN University), leading researcher at the Laboratory of Information Technologies of The Joint Institute for Nuclear Research (e-mail: bijan64@mail.ru, phone: +7(962)9095155, ORCID: https://orcid.org/0000-0002-6741-5409, ResearcherID: E-6604-2018, Scopus Author ID: 7202946069)

Rikhvitsky, Victor S. — Master of physical and mathematical Sciences, Leading programmer of the Laboratory of Information Technologies of the Joint Institute for Nuclear Research (JINR) (e-mail: rqvtsk@mail.ru, ORCID: https://orcid.org/0000-0001-6597-7443, Scopus Author ID: 57190934347)

УДК 524.834
PACS 07.05.Tp, 98.80.Es,
DOI: 10.22363/2658-4670-2020-28-2-120-130

Применение моделей Фридмана для описания эволюции Вселенной на основе данных SAI Supernovae Catalog

А. С. Гавриков[1, 2], **Биджан Саха**[1], **В. С. Рихвицкий**[1]

[1] *Институт физических исследований и технологий*
Российский университет дружбы народов
ул. Миклухо-Маклая, д. 6, Москва, 117198, Россия
[2] *Лаборатория информационных технологий*
Объединённый институт ядерных исследований
ул. Жолио-Кюри, д. 6, Дубна, Московская область, 141980, Россия

В последние годы благодаря современным и изощрённым технологиям астрономы и астрофизики смогли заглянуть вглубь Вселенной. Полученные при этом данные ставят перед космологами новые проблемы. Одна из проблем заключается в разработке адекватной и достаточной теории. Другая проблема заключается в сопоставлении теоретических результатов с результатами наблюдений. В настоящем докладе в рамках изотропной и однородной космологической модели Фридмана–Леметра–Робертсона–Уолкера (FLRW) мы изучаем эволюцию Вселенной, заполненной пылью или космологической постоянной. Причина рассмотрения этих моделей заключается в том, что нынешняя Вселенная удивительно однородна и изотропна в больших масштабах. Мы также сравниваем наши результаты с данными из каталога SAI Supernovae Catalog. Поскольку данные наблюдений даны в терминах постоянной Хаббла (H) и красного смещения (z), мы перепишем соответствующие уравнения в виде функций от z. Задача состоит в том, чтобы найти набор параметров для математической модели изотропной и однородной Вселенной, который лучше всего соответствует астрономическим данным, полученным при изучении сверхновых: звёздная величина (m), красное смещение (z).

Ключевые слова: фитирование, космология, Вселенная Фридмана, анализ данных

Research article

UDC 524.834
PACS 98.80.Cq,
DOI: 10.22363/2658-4670-2020-28-2-131-140

Spinor field in a spherically symmetric Friedmann Universe

Saha Bijan[1, 2], Evgeniy I. Zakharov[1], Victor S. Rikhvitsky[2]

[1] *Institute of Physical Research and Technology*
Peoples' Friendship University of Russia (RUDN University)
6, Miklukho-Maklaya St., Moscow, 117198, Russian Federation
[2] *Laboratory of Information Technologies*
Joint Institute for Nuclear Research
6, Joliot-Curie St., Dubna, Moscow region, 141980, Russian Federation

(received: April 18, 2020; accepted: June 30, 2020)

In recent years spinor field is being used by many authors to address some burning issues of modern cosmology. The motive behind using the spinor field as a source for gravitational field lies on the fact that the spinor field not only can describe the different era of the evolution but also can simulate different substances such as perfect fluid and dark energy. Moreover, the spinor field is very sensitive to the gravitational one and depending on the gravitational field the spinor field can react differently and change the spacetime geometry and the spinor field itself differently. This paper provides a brief description of the nonlinear spinor field in the Friedmann-Lemaitre-Robertson-Walker (FLRW) model. The results are compared in Cartesian and spherical coordinates. It is shown that during the transition from Cartesian coordinates to spherical ones, the energy-momentum tensor acquires additional non-zero non-diagonal components that can impose restrictions on either spinor functions or metric ones.

Key words and phrases: spinor field, FLRW model, Cartesian coordinates, spherical coordinates

1. Introduction

In 1998, it was found that the universe is not just expanding, but doing so with acceleration. Many hypotheses are proposed to explain this phenomenon. The most significant of them is the hypothesis of the existence of dark energy, which evenly fills the entire Universe and has a negative pressure. Some perfect liquid or scalar field is used to describe dark energy.

But there is another approach. Using the spinor field as a source of gravity. In recent years it was shown that the spinor field can give rise to a singularity-free Universe [1]–[5]. Beside this the spinor field can accelerate

the isotropization process of the initially anisotropic spacetime [3], [4], [6], [7]. Finally, the spinor field can be considered as an alternative model for dark energy [7]–[17].

Moreover, it was shown that spinor field is very sensitive to gravitational one [18] and its specific behavior in presence of the gravitational field can alter the geometry of the spacetime as well as the components of the spinor field itself [19].

This is possible due to the specific behavior of the spinor field in the presence of a gravitational field. The spinor field in cosmological models has already been considered in [3], [9], [20]. But in all these works, the spinor field is considered in Cartesian coordinates. A spinor field in spherically symmetric spaces was considered in [21]–[23].

As can be seen from all these works, non-diagonal components of the energy-momentum tensor can impose additional restrictions on either metric functions or spinor functions. In this paper we consider the spinor field in the framework of a spherically symmetric FLRW model. The results are compared with those obtained in Cartesian coordinates.

2. Basic equations

The action for a gravitational field and a nonlinear spinor field can be written as follows:

$$S(g,\psi,\overline{\psi}) = \int \left(\frac{R}{2\varkappa} + L_{sp}\right) d\Omega, \tag{1}$$

where R is a Ricci scalar, $\varkappa = 8\pi G$, G is a gravitational constant, L_{sp} is a Lagrangian for a nonlinear spinor field, which looks like this:

$$L_{sp} = \frac{i}{2}\left(\overline{\psi}\gamma^{\mu}\nabla_{\mu}\psi - \nabla_{\mu}\overline{\psi}\gamma^{\mu}\psi\right) - m\overline{\psi}\psi - F, \tag{2}$$

where m is the mass, $F = F(K)$ is the nonlinear term. The K parameter takes one of 4 values: I, J, $I+J$, $I-J$. Here $I = S^2 = (\overline{\psi}\psi)^2$ and $J = P^2 = (\overline{\psi}\gamma^5\psi)^2$.

From the expression (2), we can get the equations for the spinor field:

$$i\gamma^{\mu}\nabla_{\mu}\psi - m\psi - D\psi - i\Upsilon\gamma^5\psi = 0, \tag{3}$$

$$i\nabla_{\mu}\overline{\psi}\gamma^{\mu} + m\overline{\psi} + D\overline{\psi} + i\Upsilon\overline{\psi}\gamma^5 = 0, \tag{4}$$

where the following symbols are entered:

$$D = 2SF_K K_I = 2S\frac{dF}{dK}\frac{dK}{dI},$$

$$\Upsilon = 2PF_K K_J = 2P\frac{dF}{dK}\frac{dK}{dJ}.$$

From (2), (3) and (4) an alternative form of the Lagrangian can be obtained:

$$L = 2K\frac{dF}{dK} - F(K). \tag{5}$$

The covariant derivatives ∇_μ are defined as follows:

$$\nabla_\mu \psi = \partial_\mu \psi - \Gamma_\mu \psi, \tag{6}$$

$$\nabla_\mu \overline{\psi} = \partial_\mu \overline{\psi} + \overline{\psi}\Gamma_\mu, \tag{7}$$

where Γ_μ is a spinor affine connection that is defined as follows:

$$\Gamma_\mu = \frac{1}{4} g_{\rho\delta}\left(\frac{\partial e^{(b)}_\sigma}{\partial x^\mu} e^\rho_{(b)} - \Gamma^\rho_{\mu\sigma}\right)\gamma^\delta\gamma^\sigma, \tag{8}$$

where $e^{(b)}_\sigma$ is a system of orthogonal 4-vectors that obey the following expressions:

$$e^{(a)}_\mu e^\nu_{(a)} = \delta^\nu_\mu, \quad e^{(a)}_\mu e^\mu_{(b)} = \delta^a_b, \tag{9}$$

$$g_{\mu\nu}(x) = e^a_\mu(x) e^b_\nu(x)\eta_{ab}. \tag{10}$$

The expression for the energy-momentum tensor is as follows:

$$T^\rho_\mu = g^{\rho\nu}\overline{T}_{\nu\mu} - g^{\rho\nu}\tilde{T}_{\nu\mu} - \delta^\rho_\mu[2KF_K - F(K)], \tag{11}$$

where the following symbols are used:

$$\overline{T}_{\nu\mu} = \frac{i}{4}(\overline{\psi}\gamma_\mu\partial_\nu\psi + \overline{\psi}\gamma_\nu\partial_\mu\psi - \partial_\mu\overline{\psi}\gamma_\nu\psi - \partial_\nu\overline{\psi}\gamma_\mu\psi), \tag{12}$$

$$\tilde{T}_{\nu\mu} = \frac{i}{4}\overline{\psi}(\gamma_\mu\Gamma_\nu + \Gamma_\nu\gamma_\mu + \gamma_\nu\Gamma_\mu + \Gamma_\mu\gamma_\nu)\psi. \tag{13}$$

3. Cartesian coordinates

This section uses the following metric:

$$ds^2 = dt^2 - a^2(t)\left[dx^2 + dy^2 + dz^2\right]. \tag{14}$$

Nontrivial components of the Einstein tensor in this metric have the following form:

$$G^0_0 = -3\frac{\dot{a}^2}{a^2}, \tag{15}$$

$$G^i_j = -\left(2\frac{\ddot{a}}{a} + \frac{\dot{a}^2}{a^2}\right) \quad i,j = 1,2,3. \tag{16}$$

From metric (14), we can use (10) to find expressions for tetrads:

$$e_0^{(0)} = 1 \quad e_1^{(1)} = a(t) \quad e_2^{(2)} = a(t) \quad e_3^{(3)} = a(t). \tag{17}$$

Expressions for Γ_μ are obtained from (17) and (8):

$$\Gamma_0 = 0 \quad \Gamma_1 = \frac{\dot{a}}{2}\overline{\gamma}^1\overline{\gamma}^0 \quad \Gamma_2 = \frac{\dot{a}}{2}\overline{\gamma}^2\overline{\gamma}^0 \quad \Gamma_3 = \frac{\dot{a}}{2}\overline{\gamma}^3\overline{\gamma}^0. \tag{18}$$

From (3), (4) (6), (7) and (18) we get the equations for the spinor field:

$$i\overline{\gamma}^0\left(\dot{\psi} + \frac{3}{2}\frac{\dot{a}}{a}\psi\right) - m\psi - D\psi - i\Upsilon\gamma^5\psi = 0, \tag{19}$$

$$i\left(\dot{\overline{\psi}} + \frac{3}{2}\frac{\dot{a}}{a}\overline{\psi}\right)\overline{\gamma}^0 + m\overline{\psi} + D\overline{\psi} + i\Upsilon\overline{\psi}\gamma^5 = 0. \tag{20}$$

Non-trivial components of the energy-momentum tensor are obtained from (11), (12), (13), (18), (19) and (20):

$$T_0^0 = mS + F(K), \tag{21}$$

$$T_1^1 = F(K) - 2KF_K, \tag{22}$$

$$T_2^2 = F(K) - 2KF_K, \tag{23}$$

$$T_3^3 = F(K) - 2KF_K. \tag{24}$$

The complete system of Einstein equations looks like this:

$$3\frac{\dot{a}^2}{a^2} = 8\pi G(mS + F(K)), \tag{25}$$

$$2\frac{\ddot{a}}{a} + \frac{\dot{a}^2}{a^2} = 8\pi G(F(K) - 2KF_K). \tag{26}$$

A more detailed description of this case can be found in the work [24].

4. Spherical coordinates

A completely different situation occurs when moving from Cartesian coordinates to spherical ones. The transition is performed as follows:

$$x = r\sin(\theta)\cos(\varphi), \tag{27}$$

$$y = r\sin(\theta)\sin(\varphi), \tag{28}$$

$$z = r\cos(\theta). \tag{29}$$

The following metric is obtained from (27), (28), (29) and (14):

$$ds^2 = dt^2 - a^2(t)[dr^2 + r^2(d\theta^2 + \sin^2(\theta)d\varphi^2)]. \tag{30}$$

The nontrivial components of the Einstein tensor remain unchanged. Expressions for tetrads are obtained from (30) using (10):

$$e_0^{(0)} = 1 \quad e_1^{(1)} = a(t) \quad e_2^{(2)} = a(t)r \quad e_3^{(3)} = a(t)r\sin(\theta). \tag{31}$$

Expressions for affine connectivity are obtained from (31) and (8):

$$\Gamma_0 = 0, \tag{32}$$

$$\Gamma_1 = \frac{1}{2}\dot{a}\overline{\gamma}^1\overline{\gamma}^0, \tag{33}$$

$$\Gamma_2 = \frac{1}{2}(\dot{a}r\overline{\gamma}^2\overline{\gamma}^0 + \overline{\gamma}^2\overline{\gamma}^1), \tag{34}$$

$$\Gamma_3 = \frac{1}{2}(\dot{a}r\sin(\theta)\overline{\gamma}^3\overline{\gamma}^0 + \sin(\theta)\overline{\gamma}^3\overline{\gamma}^1 + \cos(\theta)\overline{\gamma}^3\overline{\gamma}^2). \tag{35}$$

Substituting (32), (33), (34) and (35) into (3) and (4) is obtained:

$$i\overline{\gamma}^0\dot{\psi} + i\frac{3}{2}\frac{\dot{a}}{a}\overline{\gamma}^0\psi + iU\overline{\gamma}^1\psi + iV\overline{\gamma}^2\psi - [m+D]\psi - i\Upsilon\gamma^5\psi = 0, \tag{36}$$

$$i\dot{\overline{\psi}}\overline{\gamma}^0 + i\frac{3}{2}\frac{\dot{a}}{a}\overline{\psi}\overline{\gamma}^0 + iU\overline{\psi}\overline{\gamma}^1 + iV\overline{\psi}\overline{\gamma}^2 + [m+D]\overline{\psi} + i\Upsilon\overline{\psi}\gamma^5 = 0, \tag{37}$$

where $U = 1/ar$ and $V = \cot(\theta)/2ar$. Now (11), (12), (13), (32)–(35) and (36)–(37) produce non-zero components of the energy-momentum tensor:

$$T_0^0 = mS + F(K), \tag{38}$$

$$T_1^1 = F(K) - 2KF_K, \tag{39}$$

$$T_2^2 = F(K) - 2KF_K, \tag{40}$$

$$T_3^3 = F(K) - 2KF_K, \tag{41}$$

$$T_1^0 = \frac{\cot(\theta)}{4r}A^3, \tag{42}$$

$$T_2^0 = -\frac{3}{4}A^3, \tag{43}$$

$$T_3^0 = \frac{3}{4}\sin(\theta)A^2 - \frac{1}{2}\cos(\theta)A^1, \tag{44}$$

$$T_3^1 = -\frac{\cos(\theta)}{4a}A^0. \tag{45}$$

From (15), (16) and T_0^0–T_3^1 we get the complete system of Einstein equations. For diagonal elements we have:

$$3\frac{\dot{a}^2}{a^2} = 8\pi G[mS + F(K)], \tag{46}$$

$$2\frac{\ddot{a}}{a}+\frac{\dot{a}^2}{a^2}=8\pi G[F(K)-2KF_K]. \tag{47}$$

Expressions for non-diagonal elements:

$$\frac{\cot(\theta)}{4r}A^3=0, \tag{48}$$

$$-\frac{3}{4}A^3=0, \tag{49}$$

$$\frac{3}{4}\sin(\theta)A^2-\frac{1}{2}\cos(\theta)A^1=0, \tag{50}$$

$$-\frac{\cos(\theta)}{4a}A^0=0, \tag{51}$$

where $A^\mu=\overline{\psi}\gamma^5\gamma^\mu\psi$ — components of the 4-pseudovector. This shows that the equations are identical for diagonal components, but non-diagonal components impose some additional conditions on either metric functions or spinor functions. These restrictions will be discussed in more detail in the next section. But this requires equations for spinor invariants. They are obtained from (36)–(37) and look like this:

$$\dot{S}+3\frac{\dot{a}}{a}S+2\Upsilon A^0=0,\quad \dot{P}+3\frac{\dot{a}}{a}P-2[m+D]A^0=0, \tag{52}$$

$$\dot{A}^1+3\frac{\dot{a}}{a}A^1+2UA^0=0,\quad \dot{A}^2+3\frac{\dot{a}}{a}A^2+2VA^0=0, \tag{53}$$

$$\dot{A}^0+3\frac{\dot{a}}{a}A^0+2UA^1+2VA^2+2[m+D]P-2\Upsilon S=0. \tag{54}$$

In this instance $(\gamma^5)^2=1$. The first integral of this system is equal to:

$$S^2+P^2+(A^0)^2-(A^1)^2-(A^2)^2=\frac{C}{a^6},\quad C=const. \tag{55}$$

5. Restrictions on the spinor functions

As mentioned earlier, the equations (48), (49), (50) and (51) impose restrictions on either the metric function or the spinor functions that are the solution of the equations (36)–(37). It follows from (48)–(51) that $A^3=0$ and $A^0=0$. A restriction on A^1 and A^2 looks like this:

$$A^1=\frac{3}{2}\tan(\theta)A^2. \tag{56}$$

Using (56) and equations from (48) to (51) we get the following:

$$S^2+P^2+(A^0)^2-(A^2)^2\left[\frac{9}{4}\tan^2(\theta)+1\right]=\frac{C}{a^6}. \tag{57}$$

It can also be shown [24] that if $m \neq 0$, then:

$$K = I = S^2 = \frac{C_1}{a^6}, \quad C_1 = const. \tag{58}$$

If $m = 0$, then:

$$K = \frac{C_2}{a^6}, \quad C_2 = const \tag{59}$$

for $K = I$, $K = J$, $K = I + J$ and $K = I - J$.

6. Discussion

Though there is a number of papers dealing with FLRW cosmological model with spinor fields, we did it again. Main idea was to see how the coordinate transformation effects the behavior of spacetime evolution and the spinor field. Moreover, mathematically it may help us to model different type of stars using the spinor field as a source field. In that sense this study is the beginning of the further studies that we plan to carry out in future.

7. Conclusions

Within the scope of spherically symmetric FLRW model we study the role of the spinor field in the evolution of the Universe. It is found that the usual transition from Cartesian coordinates to spherical ones leads to the appearance of non-zero non-diagonal components of the energy-momentum tensor. The presence of these components leads to some restrictions on spinor functions. However, these limitations may not always directly affect the solution of Einstein's equations. For example, if $K = I = S^2$, these restrictions will not affect the solution of the equations (25) and (26).

Acknowledgments

The publication has been prepared with the support of the "RUDN University Program 5-100" and funded by RFBR according to the research projects No. 18-07-00692 and No. 16-07-00766.

References

[1] B. Saha and G. N. Shikin, "Interacting Spinor and Scalar Fields in Bianchi Type I Universe Filled with Perfect Fluid: Exact Self-consistent Solutions," *General Relativity and Gravitation*, vol. 29, pp. 1099–1112, 1997. DOI: 10.1023/a:1018887024268.

[2] B. Saha and G. N. Shikin, "Nonlinear Spinor Field in Bianchi type-I Universe filled with Perfect Fluid: Exact Self-consistent Solutions," *Journal of Mathematical Physics*, vol. 38, pp. 5305–5318, 1997. DOI: 10.1063/1.531944.

[3] B. Saha, "Spinor field in Bianchi type-I Universe: regular solutions," *Physical Review D*, vol. 64, p. 123 501, 2001. DOI: 10.1103/physrevd.64.123501.

[4] B. Saha, "Nonlinear Spinor Field in cosmology," *Physical Review D*, vol. 69, p. 124 006, 2004. DOI: 10.1103/physrevd.69.124006.

[5] B. Saha and T. Boyadjiev, "Bianchi type-I cosmology with scalar and spinor fields," *Physical Review D*, vol. 69, p. 124 010, 2004. DOI: 10.1103/physrevd.69.124010.

[6] B. Saha, "Spinor fields in Bianchi type-I Universe," *Physics of Particlesand Nuclei.*, vol. 37, S13–S44, 2006. DOI: 10 . 1134 / s1063779606070021.

[7] N. J. Popławski, "Nonsingular, big-bounce cosmologyfrom spinor-torsion coupling," *Physical Review D*, vol. 85, p. 107 502, 2012. DOI: 10.1103/physrevd.85.107502.

[8] M. O. Ribas, F. P. Devecchi, and G. M. Kremer, "Fermions as sources of accelerated regimes in cosmology," *Physical Review D*, vol. 72, p. 123 502, 2005. DOI: 10.1103/physrevd.72.123502.

[9] B. Saha, "Nonlinear spinor field in Bianchi type-I cosmology: inflation,isotropization, and late time acceleration," *Physical Review D*, vol. 74, p. 124 030, 2006. DOI: 10.1103/physrevd.74.124030.

[10] B. Saha, "Spinor field and accelerated regimes in cosmology," *Gravitation & Cosmology*, vol. 12, no. 46–47, pp. 215–218, 2006.

[11] B. Saha, "Nonlinear spinor field in Bianchi type-I cosmology: accelerated regimes," *Romanian Reports in Physics*, vol. 59, pp. 649–660, 2007. arXiv: gr-qc/0608047.

[12] B. Saha, "Early inflation, isotropization and late-time acceleration of a Bianchi type-I universe," *Physics of Particles and Nuclei*, vol. 40, pp. 656–673, 2009. DOI: 10.1134/s1063779609050037.

[13] N. J. Popławski, "Big bounce from spin and torsion," *General Releativity and Gravitation*, vol. 44, p. 1007, 2012. DOI: 10.1007/s10714-011-1323-2.

[14] N. J. Popławski, "Nonsingular Dirac particles in spacetime with torsion," *Physics Letters B*, vol. 690, pp. 73–77, 2010. DOI: 10.1016/j.physletb.2010.04.073.

[15] L. Fabbri, "A Discussion on Dirac Field Theory, No-Go Theorems and Renormalizability," *International Journal of Theoretical Physics*, vol. 52, pp. 634–643, 2013. DOI: 10.1007/s10773-012-1370-9.

[16] L. Fabbri, "Conformal gravity with the most general ELKO matter," *Physical Review D.*, vol. 85, p. 047 502, 2012. DOI: 10.1103/physrevd.85.047502.

[17] S. Vignolo, L. Fabbri, and R. Cianci, "Dirac spinors in Bianchi-I $f(R)$-cosmology with torsion," *Journal of Mathematical Physics*, vol. 52, p. 112 502, 2011. DOI: 10.1063/1.3658865.

[18] B. Saha, "Nonlinear Spinor Fields in Bianchi type-I spacetime: Problems and Possibilities," *Astrophysics and Space Science*, vol. 357, p. 28, 2015. DOI: 10.1007/s10509-015-2291-x.

[19] B. Saha, "Spinor field nonlinearity and space-time geometry," *Physics of Particles and Nuclei*, vol. 49, no. 2, pp. 146–212, 2018. DOI: 10.1134/s1063779618020065.

[20] B. Saha, "Non-minimally coupled nonlinear spinor field in Bianchi type-I cosmology," *European Physical Journal – Plus*, vol. 134, p. 419, 2019. DOI: 10.1140/epjp/i2019-12859-7.

[21] R. Cianci, L. Fabbri, and S. Vignolo, "Exact solutions for Weyl fermions with gravity," *European Physical Journal – Plus*, vol. 75, p. 478, 2015. DOI: 10.1140/epjc/s10052-015-3698-9.

[22] K. A. Bronnikov, Y. P. Rybakov, and B. Saha, "Spinor fields in spherical symmetry. Einstein-Dirac and other space-time," *European Physical Journal – Plus*, vol. 135, p. 124, 2020. DOI: 10.1140/epjp/s13360-020-00150-z.

[23] B. Saha, "Spinor fields in spherically symmetric space-time," *European Physical Journal – Plus*, vol. 133, p. 416, 2018. DOI: 10.1140/epjp/i2018-12273-9.

[24] B. Saha, "Spinor Field Nonlinearity and Space-Time Geometry," *Physics of Particles and Nuclei*, vol. 49, no. 2, pp. 146–212, 2018. DOI: 10.1134/S1063779618020065.

For citation:

S. Bijan, E. I. Zakharov, V. S. Rikhvitsky, Spinor field in a spherically symmetric Friedmann Universe, Discrete and Continuous Models and Applied Computational Science 28 (2) (2020) 131–140. DOI: 10.22363/2658-4670-2020-28-2-131-140.

Information about the authors:

Saha, Bijan — Doctor of Physical and Mathematical Sciences, assistant professor of the Institute of Physical Research and Technologies of Peoples' Friendship University of Russia (RUDN University), leading researcher at the Laboratory of Information Technologies of The Joint Institute for Nuclear Research (e-mail: bijan64@mail.ru, phone: +7(962)9095155, ORCID: https://orcid.org/0000-0002-6741-5409, ResearcherID: E-6604-2018, Scopus Author ID: 7202946069)

Zakharov, Evgeniy I. — student of the Institute of Physical Research and Technologies of Peoples' Friendship University of Russia (RUDN University) (e-mail: zakharov.eugene1998@gmail.com, phone: +7(901)7062157, ORCID: https://orcid.org/0000-0003-2458-6109)

Rikhvitsky, Victor S. — Master of physical and mathematical Sciences, Leading programmer of the Laboratory of Information Technologies of the Joint Institute for Nuclear Research (JINR) (e-mail: rqvtsk@mail.ru, ORCID: https://orcid.org/0000-0001-6597-7443, Scopus Author ID: 57190934347)

УДК 524.834
PACS 98.80.Cq,
DOI: 10.22363/2658-4670-2020-28-2-131-140

Спинорное поле в сферически симметричной Вселенной Фридмана

Саха Биджан[1, 2], Е. И. Захаров[1], В. С. Рихвицкий[2]

[1] *Институт физических исследований и технологий*
Российский университет дружбы народов
ул. Миклухо-Маклая, д. 6, Москва, 117198, Россия
[2] *Лаборатория информационных технологий*
Объединённый институт ядерных исследований
ул. Жолио-Кюри, д. 6, Дубна, Московская область, 141980, Россия

В последние годы спинорное поле используется многими авторами для решения некоторых актуальных вопросов современной космологии. Мотив использования спинорного поля в качестве источника гравитационного поля заключается в том, что спинорное поле может не только описывать различные этапы эволюции Вселенной, но и моделировать различные типы вещества, такие как идеальная жидкость и темная энергия. Кроме того, спинорное поле очень чувствительно к гравитационному, и в зависимости от гравитационного поля спинорное поле может реагировать по-разному, изменяя тем самым геометрию пространства-времени. В настоящей работе дается краткое описание нелинейного спинорного поля в модели Фридмана–Леметра–Робертсона–Уолкера (FLRW). Результаты сравниваются в декартовых и сферических координатах. Показано, что при переходе от декартовых координат к сферическим тензор энергии-импульса имеет дополнительные ненулевые недиагональные компоненты, которые могут накладывать ограничения как на спинорные функции, так и на метрические.

Ключевые слова: спинорное поле, модель FLRW, декартовы координаты, сферические координаты

Research article

UDC 519.872:519.217
PACS 07.05.Tp, 02.60.Pn, 02.70.Bf
DOI: 10.22363/2658-4670-2020-28-2-141-153

Kinematic support modeling in Sage

Oleg K. Kroytor[1], Mikhail D. Malykh[1], Sergei P. Karnilovich[2]

[1] *Department of Applied Probability and Informatics*
Peoples' Friendship University of Russia (RUDN University)
6, Miklukho-Maklaya St., Moscow, 117198, Russian Federation
[2] *Institute for Physical Research and Technology*
Peoples' Friendship University of Russia (RUDN University)
6, Miklukho-Maklaya St., Moscow, 117198, Russian Federation

(received: May 15, 2020; accepted: June 30, 2020)

The article discusses the kinematic support, which allows reducing the horizontal dynamic effects on the building during earthquakes. The model of a seismic isolation support is considered from the point of view of classical mechanics, that is, we assume that the support is absolutely solid, oscillating in a vertical plane above a fixed horizontal solid plate. This approach allows a more adequate description of the interaction of the support with the soil and the base plate of the building. The paper describes the procedure for reducing the complete system of equations of motion of a massive rigid body on a fixed horizontal perfectly smooth plane to a form suitable for applying the finite difference method and its implementation in the Sage computer algebra system.

The numerical calculations by the Euler method for grids with different number of elements are carried out and a mathematical model of the support as a perfectly rigid body in the Sage computer algebra system is implemented. The article presents the intermediate results of numerical experiments performed in Sage and gives a brief analysis (description) of the results.

Key words and phrases: kinematic support, seismic isolation support, mathematical model, finite difference method, computer algebra system, Sage, numerical calculations

1. Introduction

As one of the types of seismic protection of buildings in seismically active regions of the Earth, among others, auxiliary "seismic suppression" supports are used. A large number of standards of such supports are known with a high level of reliability of operation and a high ability to damp seismic waves of high magnitude. They are high-tech in manufacturing, are sold at high prices and, thanks to efficiency and reliability, are in high demand among large construction companies and in areas with a high standard of living.

At the same time, in poor areas of developing countries, citizens and municipalities cannot afford to use them. However, it is precisely in such regions that residents most often suffer from the devastating effects of earthquakes. The Soviet, and then the Russian school of seismic protection architecture was able to offer inexpensive and effective solutions in the form of so-called kinematic supports.

In our country and abroad, a large number of active seismic protection systems for buildings have been proposed, developed and applied. Among them are those proposed by A. Kurzanov, S. Yu. Semenov [1], [2], Yu. P. Cherepinsky [3], V. V. Nazina, etc. Some of these systems were practically implemented in real buildings [1], [2], [4], [5], making it possible to assess their workability for building industry. Vibration tests were carried out at many facilities [6], [7], which provided experimental data on the behavior of these systems under dynamic impacts. However, essentially all developed systems need additional analysis under full-scale conditions. Therefore, many aspects of the real behavior of seismic protection systems are difficult to study theoretically or on models due to the very large number of factors affecting the behavior of the structure during an intense earthquake.

Kinematic supports are vertically placed cylinders on which the building rests. Neither the place of entry of the support into the ground or concrete slab, nor the contact with the horizontal slab of the building placed on such supports, are fixed rigidly. Supports can be made in the form of short concrete pillars with an outer cage of steel pipe or a reinforcing cage of carbon composite or basalt composite nets. It is promising to use in the construction of concrete racks with dispersed reinforcement basalt fiber, since such concretes have increased resistance to cracking and tensile strength during bending.

The essence of the kinematic support is that when the base is displaced by a certain design value, the building slightly rises, receiving some additional kinetic energy. In this case, a returning torque arises, bringing the "base-building" system to its original state (position before the earthquake). Residential buildings constructed using seismic isolating supports have full-scale confirmation of the reliability of the structure and have proven themselves successful in experimental studies [1], [2].

The aim of our work is to create an adequate mathematical model of the support and its interface with the building, which will help to design kinematic supports taking into account the operational requirements of customers.

The solution to this problem can be approached from two sides. First, it is possible to create a model of elastic support in the Ansys, system [8]. With this approach, the main difficulty is the selection of adequate boundary conditions for the place where the support is in contact with the soil and base plate of the building.

The second approach proposes to consider the support from the point of view of classical mechanics, assuming it to be a perfectly rigid body, oscillating in a vertical plane above a fixed horizontal absolutely smooth plate, but more adequately describe the interaction of the support with the ground and the building plate.

From the point of view of analytical mechanics, the motion of kinematic supports is the motion of a complex system of bodies with non-holding bonds [9]. The mathematical basis of the dynamics of such systems was developed

by outstanding mathematicians J. Dalamber, S. Poisson, Yu. A. Arkhangelsky, V. V. Kozlov, A. P. Markeev and others. In our work, we will follow the formalism developed by A. P. Markeev.

Models of rigid body mechanics are systems of a large number of ordinary differential equations (ODEs) that are not resolved with respect to derivatives [10], [11]. They, as a rule, do not allow an analytical solution. Therefore, we are going to use the finite difference method. For its successful application, it is important to solve the equations for derivatives by increasing the order. Due to the large number of equations, this procedure turns out to be rather complicated. Therefore, it seems natural to execute it in a computer algebra system (CAS). Computer-aided study of such models is carried out in two stages:

1) symbolic transformations reducing the system to normal form, used in the standard formulation of the Cauchy theorem;

2) numerical solution of this system using the finite difference method (rk4).

We chose the Sage system [12], because it can execute both the first and second stages. To test the described approach, we took the simplest model that describes the complete system of equations of motion of a massive rigid body along a fixed horizontal perfectly smooth plane [10], [11].

2. Description of the mathematical model

Let the seismic isolation support be a rigid body and have the shape of a cylinder, in which one of the bases has a spherical shape. The support is installed between the foundation of the building (a horizontal rigid plate) and the building itself. The support touches the foundation of the building always with a spherical end [13]. We assume that when oscillating or when horizontal forces act on the foundation of the structure, the point of contact of the support and the base plate always lies in the plane Oxy.

To describe the vibration of the support, we will use the model of motion of a rigid body on the surface [10], [11] and adapt this model to our task.

The motion of the body will be considered relative to the fixed laboratory coordinate frame Oxy with the origin O at a certain point of the plane. The axis Oz is directed vertically, n is the unit vector of inner normal to the body surface at point of the axis z. Let $G\xi\eta\zeta$ denote the moving coordinate frame rigidly coupled to the body with the origin at its center of gravity G and the axes directed along the principal axes of inertia 1. The orientation of the body with respect to the fixed laboratory frame is specified by the Euler angles ϕ, ψ, θ or by the matrix of direction cosines a_{ij}. The unit vector of the z-axis in the frame $G\xi\eta\zeta$ is specified by the components a_{31}, a_{32}, a_{33}:

$$a_{31} = \sin\theta\sin\phi, \quad a_{32} = \sin\theta\cos\phi, \quad a_{33} = \cos\theta.$$

Assume ξ, η, ζ to be the principal axes of inertia with respect to the gravity center. Let M be the point of contact between the horizontal plane Oxy and the support (see Figure 1). Its coordinates ξ, η, ζ in the frame $G\xi\eta\zeta$ will be functions of angles ϕ, θ, determined from the form of equation $F(\xi, \eta, \zeta) = 0$ that specifies the shape of the body surface [10], [11]. The sign of function F

is chosen such that $n = -\dfrac{\nabla F}{|\nabla F|}$. Then the quantities a_{ij} for the axis z are expressed in terms of the Euler angles as

$$\begin{cases} a_{31} = \sin\theta\sin\phi = -\dfrac{1}{|\nabla F|}\dfrac{F}{\nabla\xi}, \\ a_{32} = \sin\theta\cos\phi = -\dfrac{1}{|\nabla F|}\dfrac{F}{\nabla\eta}, \\ a_{33} = \cos\theta = -\dfrac{1}{|\nabla F|}\dfrac{F}{\nabla\zeta}. \end{cases} \tag{1}$$

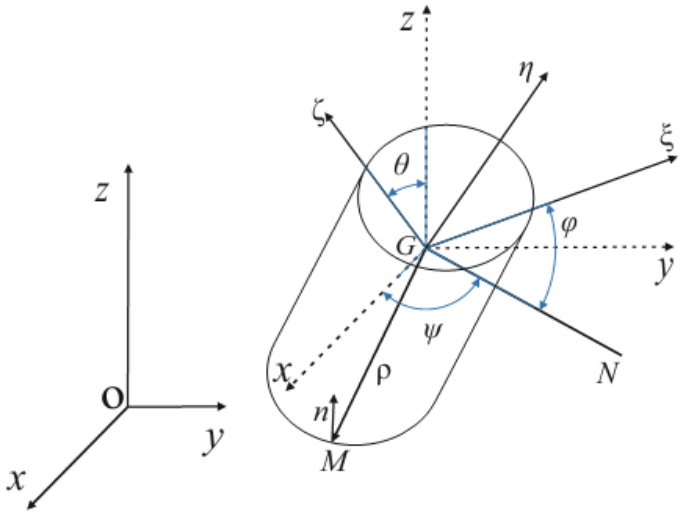

Figure 1. Motion of a perfectly rigid body above the perfectly smooth horizontal plane

Following the studies presented in Refs. [10], [11], [14], [15], let us consider the full system of equations of motion for a massive rigid body on a fixed horizontal perfectly smooth plane and introduce the following unknown functions of time t: center of gravity coordinates x, y, z of the body in the laboratory frame; Euler angles ϕ, ψ, θ; components ξ, η, ζ of radius vector ρ of point M of contact of the support and the plane (base plate) relative to the gravity center, and magnitude N of the normal reaction of the plane.

To determine the unknowns listed above the following equations and relations will be used:

a) The equations that represent the theorem of momentum variation. The external forces are the reaction of the plane $R = N \cdot n$ directed vertically ($N \geqslant 0$) and the gravity force. The equations are:

$$\begin{cases} m\ddot{x} = 0, \\ m\ddot{y} = 0, \\ m\ddot{z} = -mg + N, \end{cases} \tag{2}$$

where m is the body mass, g is the free fall acceleration.

b) The equations that represent the theorem of angular momentum variation:

$$\begin{cases} A\dfrac{dp}{dt} + (C-B)qr = N(\eta a_{33} - \zeta a_{32}), \\ B\dfrac{dq}{dt} + (A-C)rp = N(\zeta a_{31} - \xi a_{33}), \\ C\dfrac{dr}{dt} + (B-A)pq = N(\xi a_{32} - \eta a_{31}), \end{cases} \tag{3}$$

where p, q, r are the projections of the angular velocity vector ω on the axes of the coordinate system G_ξ, G_η, G_ζ rigidly bound to the body; A, B, C are the principal moments of inertia with respect to these axes.

c) The relations represented by the Euler kinematic equations:

$$\begin{cases} p = \dot{\psi}\ \sin\theta \sin\phi + \dot{\theta}\ \cos\phi, \\ q = \dot{\psi}\ sin\,\theta \cos\phi - \dot{\theta}\ \sin\phi, \\ r = \dot{\psi}\ \cos\theta + \dot{\phi}. \end{cases} \tag{4}$$

d) The Poisson equations:

$$\begin{cases} \dot{a}_{31} = a_{32}r - a_{33}q, \\ \dot{a}_{32} = a_{33}p - a_{31}r, \\ \dot{a}_{33} = a_{31}q - a_{32}p \end{cases} \tag{5}$$

indicating the fact that vector n defines an invariable direction in the fixed coordinate frame $Oxyz$;

e) The equation of the body surface in the coordinate frame rigidly bound to the body and having the origin at its center of gravity:

$$F(\xi, \eta, \zeta) = 0. \tag{6}$$

In our case, the body surface equation is the equation of a sphere (the support has spherical shape at the point of contact with the plate):

$$\xi^2 + \eta^2 + (\zeta + a)^2 = R^2. \tag{7}$$

f) The constraint equation

$$z = -\rho \cdot n = -(a_{31}\xi + a_{32}\eta + a_{33}\zeta) \tag{8}$$

means that the support moves contacting with the plate all the time. Equations and relations (1)–(8) determine a complete system of equations of motion of a massive rigid body on a fixed horizontal perfectly smooth plane that can be written in the following form:

$$\begin{cases} m\ddot{x} = 0, \\ m\ddot{y} = 0, \\ m\ddot{z} = -mg + N, \\ A\dfrac{dp}{dt} + (C-B)qr = N(\eta a_{33} - \zeta a_{32}), \\ B\dfrac{dq}{dt} + (A-C)rp = N(\zeta a_{31} - \xi a_{33}), \\ C\dfrac{dr}{dt} + (B-A)pq = N(\xi a_{32} - \eta a_{31}), \\ \dot{a}_{31} = a_{32}r - a_{33}q, \\ \dot{a}_{32} = a_{33}p - a_{31}r, \\ \dot{a}_{33} = a_{31}q - a_{32}p, \\ F(\xi,\eta,\zeta) = 0, \\ z = -\rho \cdot n = -(a_{31}\xi + a_{32}\eta + a_{33}\zeta), \\ a_{31} = \sin\,\theta\,\sin\,\phi = -\dfrac{1}{|\nabla F|}\dfrac{\partial F}{\partial \xi}, \\ a_{32} = \sin\,\theta\,\cos\,\phi = -\dfrac{1}{|\nabla F|}\dfrac{\partial F}{\partial \eta}, \\ a_{33} = \cos\,\theta = -\dfrac{1}{|\nabla F|}\dfrac{\partial F}{\partial \zeta}, \\ p = \dot{\psi}\,\sin\,\theta\sin\,\phi + \dot{\theta}\,\cos\,\phi, \\ q = \dot{\psi}\,\sin\,\theta\cos\,\phi - \dot{\theta}\,\sin\,\phi, \\ r = \dot{\psi}\,\cos\,\theta + \dot{\phi}. \end{cases} \tag{9}$$

From relation (1) and equation (7), we get explicit expressions of a_{ij} for the spherical base of a kinematic support:

$$\begin{cases} a_{31} = -\dfrac{1}{|\nabla F|}\dfrac{\partial F}{\partial \xi} = -\dfrac{1}{\sqrt{4\xi^2 + 4\eta^2 + 4(\zeta+a)^2}} \cdot 2\xi = -\dfrac{1}{R}\xi, \\ a_{32} = -\dfrac{1}{|\nabla F|}\dfrac{\partial F}{\partial \eta} = -\dfrac{1}{\sqrt{4\xi^2 + 4\eta^2 + 4(\zeta+a)^2}} \cdot 2\eta = -\dfrac{1}{R}\eta, \\ a_{33} = -\dfrac{1}{|\nabla F|}\dfrac{\partial F}{\partial \zeta} = -\dfrac{1}{\sqrt{4\xi^2 + 4\eta^2 + 4(\zeta+a)^2}} \cdot 2\zeta = -\dfrac{1}{R}(\zeta + a). \end{cases} \tag{10}$$

Using the formulae (10), is it easy to express the components ξ, η, ζ, therefore, we can get rid of the Poisson equations in the system (9), since the values of a_{ij} and components ξ, η, ζ are already known. According to the two first equations of (9), the center of gravity moves so that its projection on the base horizontal plane moves rectilinearly. Hence, it is obvious that the appropriate equations can be disregarded, too.

After a number of executed transformations and assumptions, the system (9) takes the form

$$\begin{cases} N = m\ddot{z} + mg, \\ A\dfrac{dp}{dt} + (C-B)qr = N(\eta a_{33} - \zeta a_{32}), \\ B\dfrac{dq}{dt} + (A-C)rp = N(\zeta a_{31} - \xi a_{33}), \\ C\dfrac{dr}{dt} + (B-A)pq = N(\xi a_{32} - \eta a_{31}), \\ \xi^2 + \eta^2 + (\zeta + a)^2 = R^2, \\ z = -\rho \cdot n = -(a_{31}\xi + a_{32}\eta + a_{33}\zeta), \\ a_{31} = \sin\,\theta\,\sin\,\phi = -\dfrac{1}{|\nabla F|}\dfrac{\partial F}{\partial \xi} = -\dfrac{1}{R}\xi, \\ a_{32} = \sin\,\theta\,\cos\,\phi = -\dfrac{1}{|\nabla F|}\dfrac{\partial F}{\partial \eta} = -\dfrac{1}{R}\eta, \\ a_{33} = \cos\,\theta = -\dfrac{1}{|\nabla F|}\dfrac{\partial F}{\partial \zeta} = -\dfrac{1}{R}(\zeta + a), \\ p = \dot{\psi}\,\sin\,\theta \sin\,\phi + \dot{\theta}\,\cos\,\phi, \\ q = \dot{\psi}\,\sin\,\theta \cos\,\phi - \dot{\theta}\,\sin\,\phi, \\ r = \dot{\psi}\,\cos\,\theta + \dot{\phi}. \end{cases} \tag{11}$$

Equations (11) are reduced to the form convenient for using the computer algebra system Sage, so that further simplifications and the solution of these equations will be carried out in this CAS. In the next section we investigate the solubility of this system of equations in Sage.

3. Resolving the system with respect to derivatives

The system (11) includes both differential equations and algebraic ones (relations). Let us use Sage to reduce it to a simper form. It is obvious that from the system (11) via the values of the direction cosines a_{31}, a_{32}, a_{33}, we can explicitly express variables ξ, η, ζ as follows:

$$\begin{cases} \xi = -R \cdot a_{31} = -R \cdot \sin\,\theta\,\sin\,\phi, \\ \eta = -R \cdot a_{32} = -R \cdot \sin\,\theta\,\cos\,\phi, \\ \zeta = -R \cdot a_{33} - a = -R \cdot \cos\,\theta - a. \end{cases} \tag{12}$$

Provided that ξ, η, ζ (12) and a_{31}, a_{32}, a_{33}, are known, it is possible to express the values of the function z.

Let us write in Sage the equation

$$z = -\rho \cdot n = -(a_{31}\xi + a_{32}\eta + a_{33}\zeta)$$

from system (11) and substitute into it the expressions for ξ, η, ζ and a_{31}, a_{32}, a_{33}, then function z will be represented by the following symbolic expression:

$$z = R \cdot \cos\phi^2 \cdot \sin\theta^2 + R \cdot \sin\phi^2 \cdot \sin\theta^2 + (R \cdot \cos\theta + a) \cdot \cos\theta.$$

We substitute the obtained expression of z into equation $N = m\ddot{z} + mg$ and calculate the normal reaction of the plane:

$$\begin{aligned} N = (&2 \cdot R \cdot \cos\phi^2 \cdot \cos\theta^2 \cdot \dot{\theta}^2 + 2 \cdot R \cdot \cos\theta^2 \cdot \sin\phi^2 \cdot \dot{\theta}^2 - 2 \cdot R \cdot \cos\phi^2 \cdot \sin\theta^2 \cdot \\ &\cdot \theta^2 - 2 \cdot R \cdot \sin\phi^2 \cdot \sin\theta^2 \cdot \dot{\theta}^2 + 2 \cdot R \cdot \cos\phi^2 \cdot \cos\theta \cdot \sin\theta \cdot \ddot{\theta} + 2 \cdot R \cdot \cos\theta \cdot \\ &\cdot \sin\phi^2 \cdot \sin\theta \cdot \ddot{\theta} - R \cdot \cos\theta^2 \cdot \dot{\theta}^2 + 2 \cdot R \cdot \sin\theta^2 \cdot \dot{\theta}^2 - (R \cdot \cos\theta + a) \cdot \cos\theta \cdot \\ &\cdot \theta^2 - R \cdot \cos\theta \cdot \sin\theta \cdot \ddot{\theta} - (R \cdot \cos\theta + a) \cdot \sin\theta \cdot \ddot{\theta}) \cdot m + g \cdot m. \end{aligned}$$

As soon as all quantities ξ, η, ζ, a_{31}, a_{32}, a_{33}, N, and p, q, r are explicitly expresses, we substitute them into equations 2–4 of the system (11) and of the form

$$\begin{cases} \Phi(\phi, \psi, \theta, \dot{\phi}, \ldots \ddot{\theta}) = 0, \\ \Psi(\phi, \psi, \theta, \dot{\phi}, \ldots \ddot{\theta}) = 0, \\ \Theta(\phi, \psi, \theta, \dot{\phi}, \ldots \ddot{\theta}) = 0. \end{cases} \tag{13}$$

Explicit expressions for Φ, Ψ, Θ were be found in Sage [12].

The system (13) is linear with respect to $\ddot{\phi}, \ddot{\psi}, \ddot{\theta}$. Now we resolve the obtained system of differential equations with respect to higher derivatives using the function `solve ()`. Ultimately, we arrive at the system of differential equations of the 6-th order resolved with respect to higher derivatives. The system incorporates three equations of the second order with respect to Euler angles. For further solution of the problem we have to decrease the order of the differential equations to the first one.

To reduce the order of the system of differential equations, we perform the changes $\dot{\phi} = u$, $\dot{\psi} = v$, $\dot{\theta} = w$. As a result, we get a system of six first-order differential equations.

4. Numerical experiments in SAGE

Let us implement explicit Euler method, in order to confirm the absence of errors related to transformation of data types.

The calculations by the Euler method will be performed using the grids with $N = 400, 800, 1600$ under the following initial conditions: $\phi_0 = 0.1$, $\psi_0 = 0.1$, $\theta_0 = \pi + 0.5$, $u_0 = 1.5$, $v_0 = 1.5$, $w_0 = 0$, $h = 2\pi/N$, $t = 0$, $A = 304$, $B = 304$, $C = 400$, $R = 1.5$, $a = 0.2$, $m = 500$, $g = 9.8$ where N is the number of steps; h is the step; ϕ_0, ψ_0, θ_0 are the Euler angles at the initial moment of time; u_0, v_0, w_0 are the initial velocities; A, B, C are the moments of inertia. The results obtained by the Euler method are presented in Figures 2–7. For $N = 400$ the results are plotted by dash lines, for $N = 800$ by dash-dot lines, and for $N = 1600$ by dot lines. The accuracy of the obtained results is estimated using the Richardson method (see Figures 9, 10).

Figure 8 shows graphs. The distance between the center of mass and the plane ground oscillates as it shown on Figure 8.

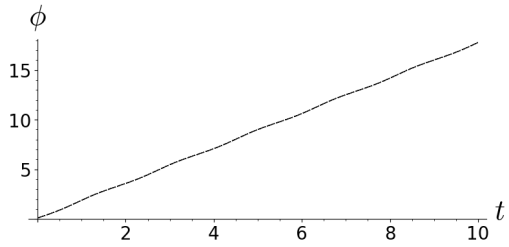

Figure 2. The angle ψ as a function of time for the grids with $N = 400, 800, 1600$

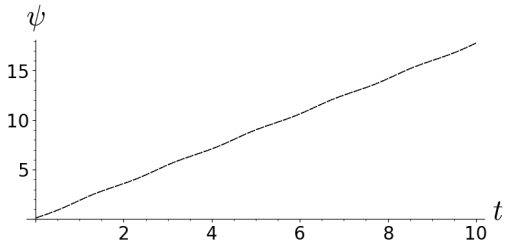

Figure 3. The angle ϕ as a function of time for the grids with $N = 400, 800, 1600$

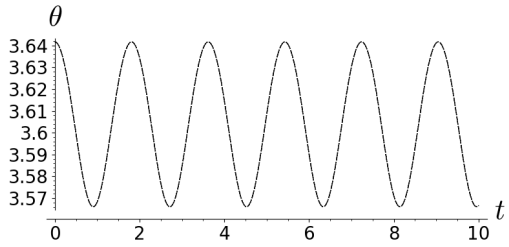

Figure 4. The angle θ as a function of time for the grids with $N = 400, 800, 1600$

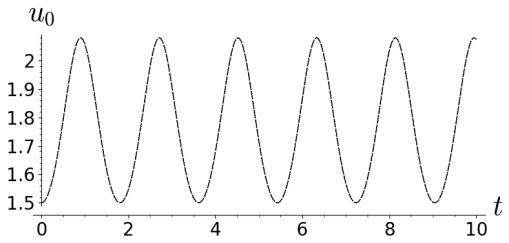

Figure 5. Rate of angle ψ change with time for the grids with $N = 400, 800, 1600$

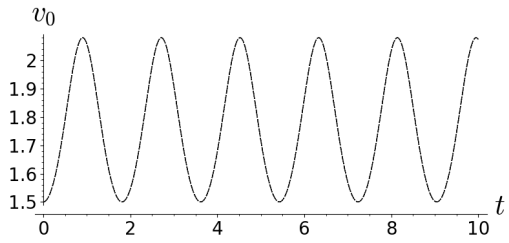

Figure 6. Rate of angle ϕ change with time for the grids with $N = 400, 800, 1600$

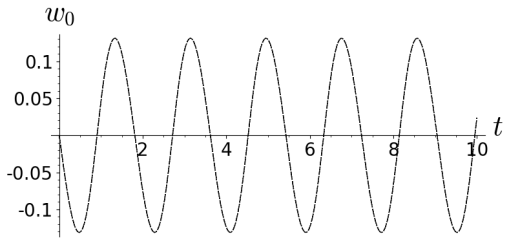

Figure 7. Rate of angle θ change with time for the grids with $N = 400, 800, 1600$

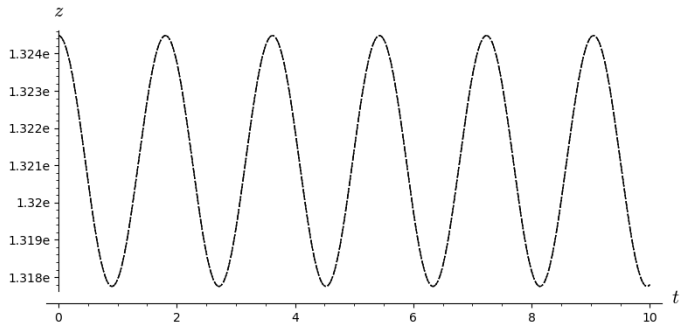

Figure 8. The center of mass height above the plane for the grids with $N = 400, 800, 1600$

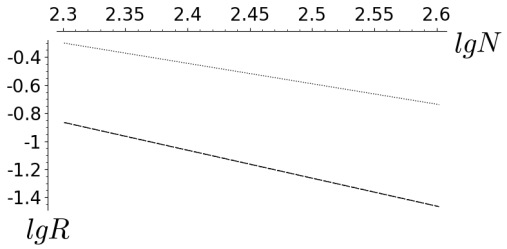

Figure 9. Accuracy of Euler solution estimated by Richardson method for the grids with $N = 400, 800, 1600$

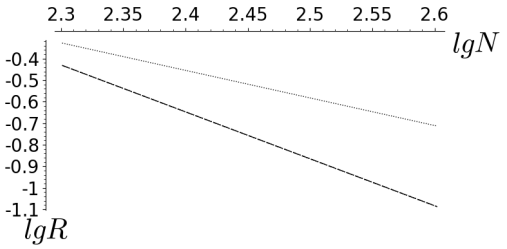

Figure 10. Accuracy of Euler solution estimated by Richardson method for the grids with $N = 400, 800, 1600$

The results obtained by the Euler method for the assumed boundary conditions show that the angles ψ, ϕ linearly increase with time (see Figures 2 and 3), while the angle θ experiences harmonic-like oscillations with growing amplitude (see Figure 4).

Figures 5–7 show that the rates of change of the Euler angles vary according to a harmonic-like law, the amplitude of oscillations increasing with time.

5. Conclusions

A crude mathematical model of a kinematic support is constructed, in which the support is considered as a perfectly rigid body oscillating in a vertical plane above a fixed horizontal perfectly smooth plate. The approximate model is rigid and does not take friction into account.

A procedure for reducing the system of differential equations of the model to a form suitable for applying the finite difference method is described and implemented in the Sage computer algebra system.

An explicit Euler method is implemented for grids with the number of partitions 400, 800, 1600 and the accuracy of the solution is estimated by the Richardson method.

For the initial and boundary conditions specified by us, the time dependence of Euler angles and their rates is determined. The results of numerical experiments are consistent with the general idea that small deviations lead to small oscillations of the support.

The problems and lines of study that will be addressed at further stages of the research are identified as follows. First, to solve the problem, we have to to determine the correct additional conditions under which the construction is stable or loses stability, i.e., when at strong ground vibrations the center of gravity horizontally shifts beyond the limits of return movement of the support and the support begins to tip over [16]. After finding the correct initial and boundary conditions, to create an adequate mathematical model of the support, we will take friction into account, specifying the reaction of the plane (base plate), and the effect of earthquakes on the movement of the supports.

Acknowledgments

The publication has been prepared with the support of the "RUDN University Program 5-100".

References

[1] A. Kurzanov and N. Skladnev, "Seismo-isolating supports for dwellings," in *Earthquake Engineering, Tenth World Conference, Balkema, Rotterdam*, 1992, pp. 1951–1954.

[2] A. M. Kurzanov and S. Y. Semenov. (2013). "Pipe-concrete seismic isolating support [Trubobetonnaya seysmoizoliruyuschaya opora]," [Online]. Available: `https://patents.google.com/patent/RU2477353C1/en1`.

[3] Y. Cherepinsky, "Seismic stability of buildings on kinematic supports," *Soil Mech Found Eng*, vol. 9, pp. 164–168, 1972. DOI: `10.1007/BF01709306`.

[4] Y. Cherepinsky, "The seismic isolation of residential buildings," *Res. Seism. Stab. Build. Struct.*, vol. 23, pp. 438–462, 2015.

[5] T. Belash, U. Begaliev, S. Orunbaev, and M. Abdybaliev, "On the Efficiency of Use of Seismic Isolation in Antiseismic Construction," *American Journal of Environmental Science and Engineering*, vol. 3, no. 4, pp. 66–74, 2019. DOI: `10.11648/j.ajese.20190304.11`.

[6] V. Smirnov, J. Eisenberg, and A. Vasil'eva, "Seismic isolation of buildings and historical monuments. Recent developments in Russia," in *13th World Conference on Earthquake Engineering. Vancouver, B.C., Canada, August 1–6*, paper no. 966, 2004.

[7] A. Uzdin, F. Doronin, G. Davydova, *et al.*, "Performance analysis of seismic-insulating kinematic foundations on support elements with negative stiffness," *Soil Mechanics and Foundation Engineering*, vol. 46, pp. 99–107, 2009. DOI: `10.1007/s11204-009-9052-1`.

[8] O. Kroytor, "The penetration modeling of flat obstacles in Ansys Autodyn program," *IOP Conference Series: Materials Science and Engineering*, vol. 675, p. 65, 2019. DOI: `10.1088/1757-899X/675/1/012027`.

[9] J. Awrejcewicz, "Kinematics of a Rigid Body and Composite Motion of a Point," in *Classical Mechanics. Advances in Mechanics and Mathematics.* May 2012, pp. 263–399. DOI: `10.1007/978-1-4614-3791-8_5`.

[10] A. Markeev, "On the theory of motion of a rigid body with a vibrating suspension," *Doklady Physics*, vol. 54, pp. 392–396, 2009. DOI: 10.1134/S1028335809080114.

[11] A. Markeev, "On the motion of a heavy dynamically symmetric rigid body with vibrating suspension point.," *Mechanics of Solids*, vol. 47, pp. 373–379, 2012. DOI: 10.3103/S0025654412040012.

[12] (2013). "SageMath, the Sage Mathematics Software System (Version 9.0.1), ReleaseDate:2020-02-20," [Online]. Available: https://www.sagemath.org.

[13] K. Bissembayev, A. Jomartov, A. Tuleshov, and T. Dikambay, "Analysis of the Oscillating Motion of a Solid Body on Vibrating Bearers," *Machines*, vol. 7, no. 3, p. 58, 2019. DOI: 10.3390/machines7030058.

[14] A. Markeev, "On the dynamics of a rigid body carrying a material point," *Regular and Chaotic Dynamics*, vol. 17, pp. 234–242, 2012. DOI: 10.1134/S1560354712030021.

[15] A. P. Markeyev, "The equations of the approximate theory of the motion of a rigid body with a vibrating suspension point," *Journal of Applied Mathematics and Mechanics*, vol. 75 (2), pp. 132–139, 2011. DOI: 10.1016/j.jappmathmech.2011.05.002.

[16] S. Karnilovich, K. Lovetskiy, L. Sevastianov, and E. Shchesnyak, "Seismic stability of oscillating building on kinematic supports," *Discrete and Continuous Models and Applied Computational Science*, vol. 27, no. 2, pp. 124–132, 2019. DOI: 10.22363/2658-4670-2019-27-2-124-132.

For citation:

O. K. Kroytor, M. D. Malykh, S. P. Karnilovich, Kinematic support modeling in Sage, Discrete and Continuous Models and Applied Computational Science 28 (2) (2020) 141–153. DOI: 10.22363/2658-4670-2020-28-2-141-153.

Information about the authors:

Kroytor, Oleg K. — Postgraduate of Department of Applied Probability and Informatics of Peoples' Friendship University of Russia (RUDN University) (e-mail: kroytor_ok@pfur.ru, phone: +7(495)9550927, ORCID: https://orcid.org/0000-0002-5691-7331)

Malykh, Mikhail D. — Doctor of Physical and Mathematical Sciences, assistant professor of Department of Applied Probability and Informatics of Peoples' Friendship University of Russia (RUDN University) (e-mail: malykh_md@pfur.ru, phone: +7(495)9550927, ORCID: https://orcid.org/0000-0001-6541-6603, ResearcherID: P-8123-2016, Scopus Author ID: 6602318510)

Karnilovich, Sergei P. — assistant professor, Ph. d., assistant professor of Institute of Physical Research and Technology of Peoples' Friendship University of Russia (e-mail: karnilovich_sp@pfur.ru, phone: +7(495)434-42-12, ORCID: https://orcid.org/0000-0001-5696-1546, Scopus Author ID: 505797810)

УДК 519.872:519.217
PACS 07.05.Tp, 02.60.Pn, 02.70.Bf
DOI: 10.22363/2658-4670-2020-28-2-141-153

Моделирование кинематических опор в Sage

О. К. Кройтор[1], **М. Д. Малых**[1], **С. П. Карнилович**[2]

[1] *Кафедра прикладной информатики и теории вероятностей*
Российский университет дружбы народов
ул. Миклухо-Маклая, д. 6, Москва, 117198, Россия
[2] *Институт физических исследований и технологий*
Российский университет дружбы народов
ул. Миклухо-Маклая, д. 6, Москва, 117198, Россия

В статье рассмотрена кинематическая опора, которая позволяет снижать горизонтальные динамические воздействия на здание во время землетрясений.

Модель сейсмоизолирующей опоры рассматривается с точки зрения классической механики, то есть предполагается, что опора — абсолютно твёрдое тело, колеблющееся в вертикальной плоскости над неподвижной горизонтальной твёрдой плитой. Данный подход позволяет более адекватно описать взаимодействие опоры с грунтом и плитой здания.

В работе описана процедура сведения полной системы уравнений движения тяжёлого твёрдого тела по неподвижной горизонтальной абсолютно гладкой плоскости к виду, пригодному для применения метода конечных разностей, и её реализация в системе компьютерной алгебры Sage.

Проведены численные расчёты методом Эйлера для сеток с разным количеством разбиений и реализована математической модель опоры как абсолютно твёрдого тела в системе компьютерной алгебры Sage. В статье представлены промежуточные результаты численных экспериментов, полученных в Sage, и дан краткий анализ (описание) результатов.

Ключевые слова: кинематическая опора, сейсмоизолирующая опора, математическая модель, МКР, система компьютерной алгебры, Sage, численные расчёты